https://doi.org/10.5194/egusphere-2026-3050
Preprint. Discussion started: 30 June 2026

Launch Emission Assessment Tool (LEAT v1.0): Part I - Development of a tool to calculate altitude-dependent rocket launch emissions for use in chemistry-climate models

Jan-Steffen Fischer[1], Stefanos Fasoulas[1], Matthias Nützel[2,3], and Anja Schmidt[2,3]

[1]University of Stuttgart, Institute of Space Systems, Stuttgart, Germany
[2]Meteorologisches Institut München, Ludwig-Maximilians-Universität München, Munich, Germany
[3]Deutsches Zentrum für Luft- und Raumfahrt, Institut für Physik der Atmosphäre, Oberpfaffenhofen, Germany

Correspondence: Jan-Steffen Fischer (fischerj@irs.uni-stuttgart.de)

Abstract. Rocket launches generate gaseous and particle emissions throughout all layers of the atmosphere, affecting both Earth's atmospheric composition and radiative balance. Emissions caused by rocket launches depend on the propellant, launch vehicle, and atmospheric conditions. To assess the atmospheric effects of rocket launch emissions, comprehensive chemistry-climate models are needed, which rely on emission inventories. These inventories need to provide detailed information on the mass profile of burned propellant in space and time, as well as the amount and chemical species emitted. However, existing emission inventories typically assume simplified burn profiles and all but one neglect the altitude dependence of post-combustion. Furthermore, the dependence of chemical reactions on engine specifics — such as engine cycle, mixture ratio, and nozzle shape — are not considered. This leads to uncertainties in the associated effects on atmospheric composition and climate.

We therefore developed the launch emission assessment tool (LEAT v1.0), which allows the calculation of both the trajectory and the emission mass based on specific vehicle parameters such as the mass, staging, and geometry of the launch vehicle, as well as the propellants and engine specifics. In this paper, the underlying models and methods used for the launch trajectory and emission calculation are presented. Using LEAT, we show that launch emissions depend strongly on the launch vehicle type, engine parameters and the assumed in-mixing of ambient air during post-combustion, which determines the altitude-dependent afterburning efficiency.

We also discuss different methods to calculate rocket launch emissions and compare results for selected rocket launch case studies, focusing on the calculation of the mass profile, the exhaust at nozzle exit level and final emissions after post-combustion within the atmosphere. Results from LEAT are compared with flight data for trajectories and common literature approaches for emissions. The approach also considers emissions of minor species such as OH, H_2, and NO_2 which are not yet covered by existing inventories but might affect atmospheric composition. Our results show that emissions of minor species are highly dependent on the chosen post-combustion efficiency. LEAT can be used to create a global, vehicle- and launch-specific rocket launch emission inventories. Additionally, uncertainties in rocket launch emissions can also be estimated. Overall, this will enable comprehensive assessments of the atmospheric effects from rocket launches using chemistry-climate models including a detailed uncertainty characterization.

https://doi.org/10.5194/egusphere-2026-3050
Preprint. Discussion started: 30 June 2026

1 Introduction

The number of space launches has grown by more than 22% per year in recent years, from 102 launch attempts in 2019 to 329 in 2025 (McDowell, 2026). Strong growth is also expected for the future (Daehnick et al., 2023). Depending on the propellant used, rocket launches emit various gaseous species and particles into the atmosphere (Sirieys et al., 2022), which affect on Earth's radiative budget (e.g. Ross et al., 2010; Ross and Sheaffer, 2014; Ryan et al., 2022; Maloney et al., 2022, 2025) and atmospheric composition (e.g. Murphy et al., 2023; Maloney et al., 2022). Despite a couple of recent studies (e.g. Ross et al., 2010; Ross and Sheaffer, 2014; Maloney et al., 2022; Ryan et al., 2022; Barker et al., 2024; Vliex et al., 2026), the analysis of the effects of emissions from rocket launches has not yet played a major role in chemistry–climate modelling until very recently. Studies from the 1990s and early 2000s — mainly analysing rocket launch–induced ozone depletion — found minor global effects at the launch rates of that time (Ross et al., 1997; Bennett and McDonald, 1998; Popp et al., 2002).

Against this background, the question arises as to what extent emissions from launches affect the atmosphere and, as a result, climate and ozone. The World Meteorological Organization (WMO) warns in its recent Scientific Ozone Assessment (World Meteorological Organization (WMO), 2022): "*Heightened concerns about influences on 21st century ozone include impacts of: [...] increased frequency of civilian rocket launches*" (World Meteorological Organization (WMO), 2022). Therefore, considering launch emissions is necessary for global atmospheric modelling. The first step to assess the effects of rocket launch emissions in climate models is the process of creating reliable and suitable launch emission inventories. To date, there has been, and partly still is, a lack of high-quality emission data for chemistry-climate modelling. As a result, apart from challenges in simulating the effects of rocket launch emissions, the input data (i.e. the emissions) themselves are already subject to uncertainties. Furthermore, the consideration of launch emissions in the assessment of environmental impacts for life cycle assessment and resulting eco-design has thus far represented a gap in the design of launch systems.

Rocket launch emissions depend on three factors: (i) The launch vehicle trajectory, which determines the mass profile of emissions over time, altitude and global position. The trajectory itself is dependent upon the specifications of the system (mass, staging, gravity turn), atmospheric conditions and further system-specific parameters. (ii) The exhaust at the nozzle exit is dependent on engine and nozzle parameters and chemical processing within the nozzle, which in turn depends on the propellants and their mass ratio, combustion pressure and nozzle expansion ratio. (iii) The extent of post-combustion behind the nozzle exit plane, which is determined by rocket geometry, velocity, altitude and atmospheric density.

In recent years, some progress has been made in the modelling of rocket launches and their emission profiles (Ross and Sheaffer, 2014; Ryan et al., 2022; Pradon et al., 2023; Barker et al., 2024; Vliex et al., 2026). These models are based on fixed trajectories except for Pradon et al. (2023), i.e. they are mostly independent of the launch vehicle specifications, while some studies use at least a stage-dependent approach (Barker et al., 2024; Brown et al., 2024; Vliex et al., 2026). Furthermore, mostly altitude-independent emission indices are used, except for Barker et al. (2024) and Vliex et al. (2026). This means that the change in post-combustion efficiency - which depends, e.g. on the available atmospheric oxygen at a certain altitude - is not

https://doi.org/10.5194/egusphere-2026-3050
Preprint. Discussion started: 30 June 2026

considered. None of the currently available emission inventories features an emission calculation that depends on the combined effect of individual launch trajectories, engine specifications and variable post-combustion efficiency.

For this reason, the Launch Emission Assessment Tool (LEAT) (Fischer et al., 2026) was developed. LEAT offers the possibility to calculate trajectories for specific launch vehicles and launch conditions (date, location, etc.). Alternatively, user-defined trajectories can be used as input. Furthermore, LEAT can calculate rocket launch emissions using one of three approaches: (i) literature-based emission indices, or explicit calculation via (ii) CEA (Gordon and McBride, 1994) or (iii) Cantera (Goodwin et al., 2024). The last two enable calculations that account for engine-specific post-combustion effects, which cause altitude-dependent variations in emissions and the formation of thermal NOx in rocket exhaust gases. Based on the trajectories and the emission calculation, a final emission profile is produced.

This paper presents the underlying theory and implementation of trajectory and emission modelling to obtain mass profiles, engine exhaust data and final emission profiles. First, the required background on terminology, trajectory, rocket plumes and emission calculation approaches is discussed within Sect. 2. The model description of LEAT is presented in Sect. 3. The sensitivity of trajectories and final emissions to the choice of modelling parameters is analysed for a few representative case studies in Sect. 4. Within this section an evaluation of trajectory results derived from LEAT using data from video streams of Falcon , Starship, and Ariane 6 is shown. This is followed by an analysis of exhaust and emission data derived from LEAT and a comparison with emission index values derived from the currently most sophisticated approach in the literature by Barker et al. (2024). A more detailed analysis of the uncertainties will be provided in a second part of this paper. Finally, we discuss our results (Sect. 5) and present our conclusions (Sect. 6).

2 Overview of methods to calculate rocket launch emissions

Dedicated rocket launch emission inventories are intended to serve chemistry–climate modelling as readily usable input data while relying on engineering knowledge. Therefore, interdisciplinary research with a common terminology is required. To produce realistic rocket launch emission inventories for use in chemistry–climate models, the location and time as well as the emission flux and emitted species must be determined. This requires coupling a model for the calculation of rocket launch trajectories with a rocket emission calculation model. Therefore, the characteristics of ascent trajectories and rocket exhaust plumes are discussed. Subsequently, methodological approaches for calculating the composition of rocket launch exhaust are presented. The implementation of these processes within LEAT is described in Sect. 3.

2.1 Rocket staging and propellant combinations

A rocket normally consists of several stages stacked on top of each other. The stage that is ignited first during launch is referred to as the “core stage”, also known as the “main stage”. Subsequent stages above it are called “upper stages”. Some rockets have additional “booster stages” ignited in parallel with the core stage, which provide additional thrust at the beginning of the ascent. The stages and boosters are jettisoned one by one during the flight to reduce the mass that needs to be accelerated. In this paper, we calculate rocket launch emissions for different case studies (i.e. launch systems using different propellant combinations)

https://doi.org/10.5194/egusphere-2026-3050
Preprint. Discussion started: 30 June 2026

and compare our results with literature-based values. The main propellant combinations typically used by launch systems are shown in Tab. 1. When talking about propellants, this refers to the combination of fuel and oxidizer. Solid propellant refers to the state of matter of both components, whereas hybrid propellants have a liquid oxidizer and a solid fuel. Currently, there are six main propellant combinations used for rocket engines (Messerschmid and Fasoulas, 2017):

- **Hydrogen:** Liquid oxygen (LOX) combined with liquid hydrogen (LH_2) is mainly used for core and upper stages. It has the advantage of a high specific impulse, which makes it attractive for upper stages. Under stoichiometric conditions, this propellant emits only water.

- **Kerosene:** The most commonly used propellant for rockets is liquid oxygen combined with kerosene, a complex hydrocarbon consisting of various long-chain hydrocarbon compounds. Furthermore, some kerosene contains residues such as sulphur. A more highly refined form of kerosene is Rocket Propellant 1 (RP-1). Here, the calculations are performed using the chemical formula $C_1H_{1.95}$. The stoichiometric combustion of kerosene leads to carbon dioxide and water vapour emissions. Kerosene is used in core and upper stages as well as for boosters.

- **Methane:** Liquid methane (LCH_4) with liquid oxygen has only recently been used as a rocket propellant. Assuming stoichiometric combustion, this propellant produces only carbon dioxide and water as emission products. Methane is used for core and upper stages and is becoming more and more important with, e.g., its use as the propellant for Starship.

- **Hypergolic:** Another propellant combination is hydrazine with dinitrogen tetroxide (NTO, N_2O_4) as the oxidizer. It has been used for core and upper stages of Russian and Chinese launchers, and also for satellites. Hydrazine is used in its simple form (N_2H_4), as unsymmetrical dimethylhydrazine (UDMH, $C_2H_8N_2$) or monomethylhydrazine (MMH, CH_6N_2). A special form used in space applications is Aerozine 50 (50% UDMH, 50% hydrazine) and UH 25 (75% UDMH, 25% hydrazine). In addition to carbon dioxide and water, the stoichiometric emission products also contain nitrogen species such as nitrogen oxides.

- **Solid:** Solid propellants are used in boosters, but also in staged engines. These can consist of different combinations. The most common is ammonium perchlorate (AP, NH_4ClO_4), which decomposes under heat into nitrogen, water, HCl and oxygen. Aluminium is also added, which reacts stoichiometrically to form aluminium oxide (Al_2O_3). Hydroxyl-terminated polybutadiene (HTPB) or polybutadiene acrylonitrile (PBAN) is used as a binder. Under stoichiometric conditions, these emit carbon dioxide, water and, in the case of PBAN, also nitrogen. Solid propellants are mainly used for booster stages, but there are also launchers where a core or upper stage contains solid propellants.

- **Hybrid:** In addition to liquid and solid fuels, hybrid fuels are also used. Currently, this is HTPB, paraffin wax or other complex hydrocarbons in combination with dinitrogen tetroxide or oxygen. This propellant combination leads to stoichiometric emissions of carbon dioxide, water and nitrogen (only in combination with N_2O_4).

https://doi.org/10.5194/egusphere-2026-3050
Preprint. Discussion started: 30 June 2026

Table 1. Main propellant combinations with their composition of oxidizer and fuel (for liquid and hybrid propellants) considered in this paper. Common abbreviations are given in brackets. Main emissions derived from stoichiometric combustion are shown as well as minor emission from incomplete combustion and post-combustion. LEAT is able to calculate emissions for more propellants.

Propellant	**Oxidizer**	**Fuel**	**Main emission products**	**Minor emission products (not exhaustive)**
Hydrogen	O_2 (LOX)	H_2	H_2O	H_2, OH, NO
Kerosene	O_2 (LOX)	RP-1	H_2O , CO_2	H_2, OH, CO, BC, NO
Methane	O_2 (LOX)	CH_4	H_2O , CO_2	H_2, OH, CO, BC, NO
Hypergolic	N_2O_4 (NTO)	$C_2H_8N_2$ or CH_6N_2	H_2O , CO_2	H_2, OH, CO, BC, NO
Solid	NH_4ClO_4, Al and HTPB or PBAN		H_2O , CO_2 , N2, Al_2O_3, HCl	H_2, OH, CO, BC, NO, Cl
Hybrid	N_2O_4 (NTO)	HTPB	H_2O , CO_2 , N_2	H_2, OH, CO, BC, NO

An overview of the aforementioned propellants and their combustion products is summarised in Tab. 1, where emissions that occur from stoichiometric combustion are referred to as “main emission species”, whereas “minor emission species” only occur in more complex combustion calculations. In this paper, we distinguish between “exhaust” which refers to conditions at the engine nozzle exit and "emission" which refers to the state after the plume interaction with the atmosphere (as, e.g., proposed by Ross et al. (2009)). In addition to the combustion products, NO is produced via thermally induced reactions of ambient nitrogen and oxygen. Furthermore, the formation of black carbon (BC, also referred to as soot) due to incomplete combustion of hydrocarbons is expected. Nearly all of these species have a direct (e.g. CO2, H2O, BC, see Ross et al., 2010; Ross and Sheaffer, 2014; Ryan et al., 2022; Barker et al., 2024, 2026; Maloney et al., 2022, 2025) or indirect effect (e.g. NOx, H2, CO,..., see Lee et al., 2021; Ocko and Hamburg, 2025) on the radiative balance. Potentially, also effects on cloud formation (see e.g. Stevens et al., 2003, 2005; Voigt et al., 2016) and their impact on on the radiation budget as well as the effects from Al_2O_3 (see e.g. Maloney et al., 2025; Ross and Sheaffer, 2014; Jain et al., 2023; Weisenstein et al., 2015) are discussed. Furthermore rocket emissions can alter ozone chemistry (e.g. most notably chlorine emissions or NOx, HOx, BC emissions; Ross et al., 1997; Ryan et al., 2022; Barker et al., 2024, 2026; Maloney et al., 2022). We therefore focus on these emissions in this paper.

2.2 General approach for calculation of emission profiles

Emission profiles show the distribution of emissions in the dimensions of time, altitude, longitude, and latitude. To generate these emission datasets, first a mass profile must be calculated using a trajectory model. This represents the distribution of the emission mass without specifying the chemical species. The mass profile derived from the trajectory contains information on where and when (time, altitude, latitude and longitude) how much propellant (mass flow) was emitted. In the next step, emissions are calculated based on the given trajectory and mass profile in the emission calculation. As a result, an emission index is calculated, containing the emission species as well as their relative mass fractions.

https://doi.org/10.5194/egusphere-2026-3050
Preprint. Discussion started: 30 June 2026

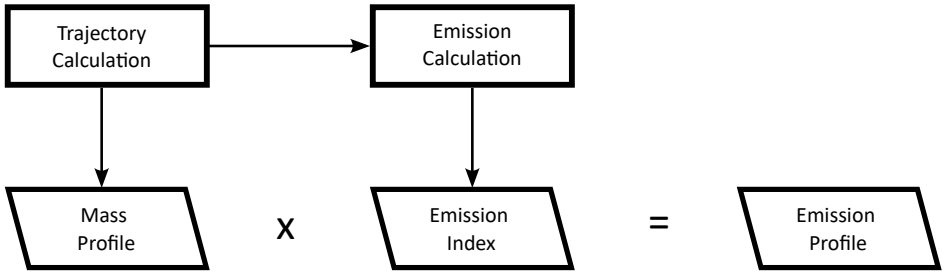

Figure 1. General approach for emission profile calculation based on the mass profile and emission index. The mass profile derived from trajectory calculations contains information on mass flow, latitude, longitude, altitude and time of propellant exhaust. The emission index derived from emission calculation contains the emission species and mass share for each step in the mass profile. When multiplied, they yield the emission profile containing emission mass and species along with their corresponding altitude, latitude, longitude, and time.

The emission index is then multiplied with the mass profile to obtain the final emission profile containing time, altitude, latitude and longitude as well as the emitted mass for each species. This process is illustrated in Fig.1.

2.3 Rocket plumes and rocket plume emissions

For the calculation of final rocket launch emissions, it is essential to understand the relevant parameters and uncertainties of the trajectory, the different phases of rocket combustion, and plume interaction with the surrounding atmosphere. Figure 2 shows the phases, parameters, and uncertainties involved in the calculation.

a) Combustion chamber

The oxidizer and fuel are mixed together and burned in the combustion chamber. Characteristic variables are the pressure in the combustion chamber p_c, the oxidizer-to-fuel mass ratio for liquid engines or propellant component mass ratio for solid engines ROF and the length of the chamber l^*. There is a variety of injector designs (e.g. showerhead, impingement, swirl, see Sutton and Biblarz, 2017; Huzel and Huang, 1992), which influence the propellant local mixing within the combustion chamber. A deviating mixing ratio can occur locally, from fuel-rich (more fuel than oxidizer can react with) to stoichiometric (enough fuel and oxidizer that can react completely with each other) combustion. Engines are typically have a fuel-rich mixing ratio for technical and performance reasons. Therefore it can be assumed that oxidizer-rich combustion does not occur. The combustion chamber geometry also plays a role in the extent to which the propellants mix and the time available for combustion. Depending on the cooling concept of the combustion chamber, film cooling is also used on the walls to protect the walls from the hot gases by an additional cold fuel film. The combustion rate and temperature distribution in rocket combustion chambers is therefore inhomogeneous, which poses a major challenge in exhaust and final emission calculation. Consequently, the formation of black carbon can also occur in the chamber by fuel-rich combustion or the cooling film. The hot gases are accelerated towards the nozzle throat before entering the nozzle.

https://doi.org/10.5194/egusphere-2026-3050
Preprint. Discussion started: 30 June 2026

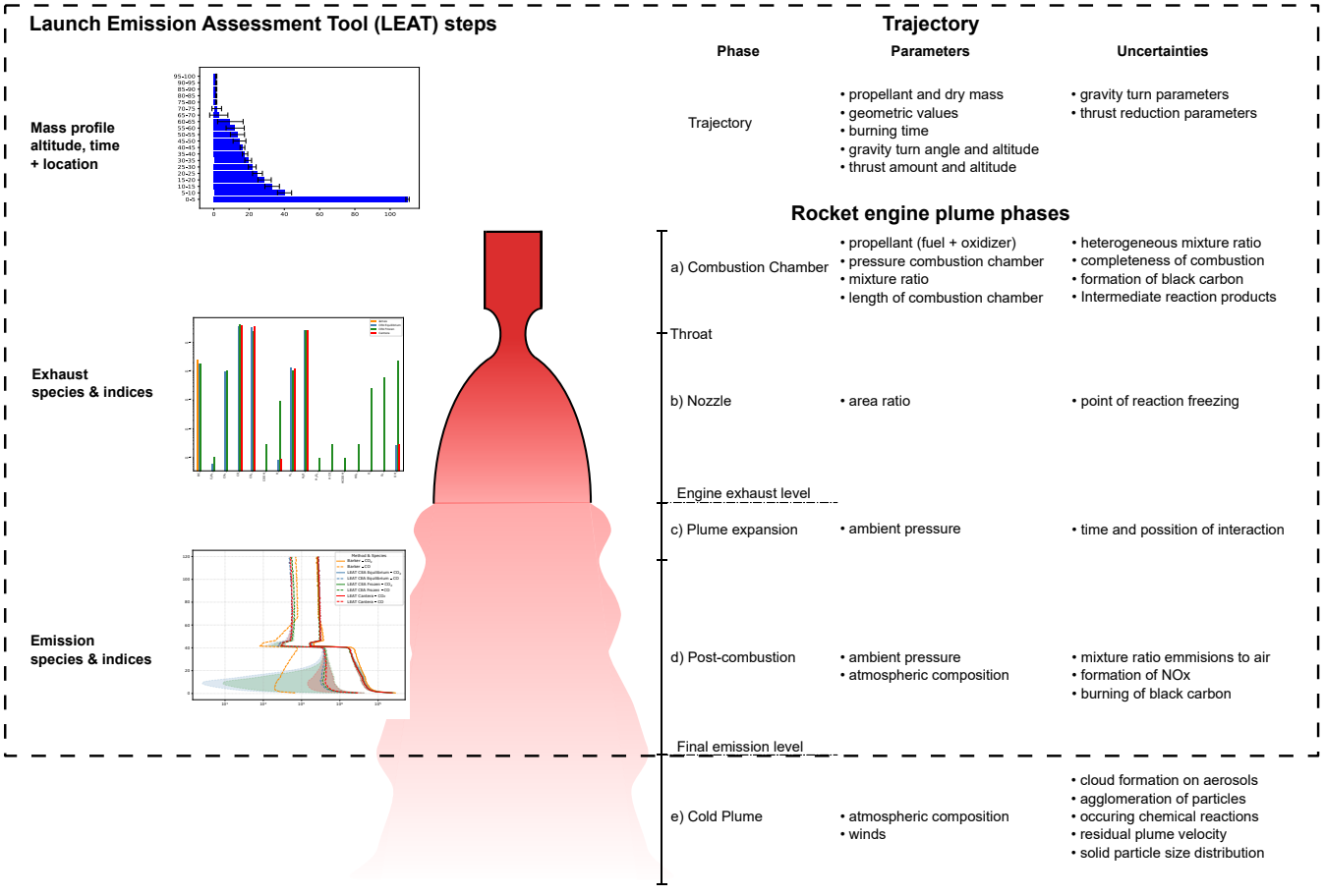

Figure 2. Schematic overview of the rocket engine plume regime phases and representation within LEAT shown on the left (dashed line represents system boundary). LEAT calculates the mass profile, exhaust at engine nozzle exit and final emission after post-combustion shown on the left schematically. On the right, the influencing parameters and uncertainties of the trajectory and phases are shown. Details of the phases are explained in the text. Scale not representative.

Furthermore, there are different engine cycles (Sutton and Biblarz, 2017; Huzel and Huang, 1992). Depending on the cycle, there might be one or more gas generators or pre-combustion chambers that produce hot gases to drive the turbopumps which feed the propellant and pressurize it. In the gas generator(s), the gases are burned either fuel-rich or oxidizer-rich and then discharged into the combustion chamber (main flow/closed cycle) or directly into the environment (bypass flow/open cycle). In the case of solid propellants, the propellant burns depending on the grain geometry. In most cases, combustion takes place in a central cavity. Hybrid engines work in a similar way, where an oxidizer stream is passed through the solid propellant and reacts with the propellant on the surface. Depending on the design, hybrid and solid propellant engines also have a post-combustion chamber in which the substances have additional time to react. The hot gases are then accelerated towards the nozzle throat.

https://doi.org/10.5194/egusphere-2026-3050
Preprint. Discussion started: 30 June 2026

b) Nozzle

Rocket nozzles are used in a variety of shapes and exit areas. They are characterized by the ratio of the nozzle end area A_e to the nozzle throat area A_t by

$$\varepsilon = \frac{A_e}{A_t}. \tag{1}$$

The higher ε, the more the gases are expanded in the nozzle, thus defining whether the nozzle is optimized for flight inside the atmosphere or outside. In the nozzle, the gases still have time to react with each other, but interactions between gas species are reduced due to the lowering pressure and associated cooling. Depending on the rocket nozzle design, the nozzle walls can also be actively cooled by fuel. Furthermore, some engines feed exhaust gases from the gas generator into the exhaust gas flow.

c) Plume expansion

After the nozzle, the gases interact with the surrounding atmosphere for the first time. Depending on the ambient pressure and the expansion rate of the nozzle which defines the pressure level at the nozzle exit, the exhaust jet is initially compressed (overexpansion) or expands (underexpansion) upon leaving the nozzle. As part of this expansion, the pressure in the exhaust jet adapts to the ambient pressure. Overexpansion usually occurs in lower atmospheric layers, as nozzles are typically designed for a specific pressure during flight. Underexpansion, on the other hand, occurs during the rest of the flight. When the altitude increases during the ascent and the ambient pressure decreases, the exhaust jet continues to expand. At high altitudes, the jet expanded in this way can also become larger in diameter than the rocket itself, so that the air deflected by the rocket can interact with the exhaust jet.

d) Post-combustion

Initially, the exhaust gas stream only begins to mix with the surrounding atmosphere at the boundary layers. This brings oxygen into contact with the mostly fuel-rich exhaust gas flow, leading to post-combustion (often referred to as afterburning). The mixing and turbulent deceleration also leads to a conversion of kinetic energy into thermal energy, which increases the temperature in addition to combustion. This can also lead to the formation of thermal nitrogen oxides. As the process continues, the entire exhaust gas jet mixes with the surrounding air such that no isolated core stream remains. This leads to further post-combustion of the fuel-rich exhaust gas jet in the interaction with the atmosphere. Due to mixing, the exhaust jet cools progressively until combustion no longer occurs and the plume velocity decreases. The mixing rate depends on the ambient atmospheric density. It can therefore be assumed that with increasing altitude, the exhaust plume no longer significantly interacts and the engine exhaust is directly emitted in phase c) with negligible post-combustion.

e) Cold plume

After cooling and deceleration, thermally induced reactions with the atmosphere no longer take place. Instead, general atmospheric chemical processes occur. The plume now moves with the surrounding atmosphere depending on the wind and is gradually mixed into the atmosphere by diffusion.

https://doi.org/10.5194/egusphere-2026-3050
Preprint. Discussion started: 30 June 2026

2.4 Ascent trajectory calculation

Calculating rocket trajectories first requires a thorough understanding of the governing forces and variables. For the trajectory calculation, we use the equations of motion given by Messerschmid and Fasoulas (2017). They represent a simplified approach, assuming $\alpha \approx 0$ as this condition is targeted during rocket ascent from Earth's surface with R_0. Fig. S1 in the supplementary material shows the applied forces.

$$\frac{\delta v}{\delta t} = \frac{F - D}{m} - g \sin(\gamma) \tag{2}$$

$$\frac{\delta x}{\delta t} = v \cos(\gamma) \tag{3}$$

$$\frac{\delta z}{\delta t} = v \sin(\gamma) \tag{4}$$

$$\frac{\delta \gamma}{\delta t} = \left(\frac{v}{R_0 + z} - \frac{g}{v} \right) \cos(\gamma) \tag{5}$$

D = Drag [N]
F = Thrust [N]
g = Gravitational acceleration [m/s^2]
L = Lift [N]
m = Mass of total system [kg]
v = Flight path velocity [m/s]
x = Downrange [m]
z = Altitude [m]
α = Angle of attack [°]
γ = Flight path angle [°]

The drag (D) of a rocket depends on the velocity v, air density ρ_a, reference area A_d, and drag coefficient c_d, and is calculated using the equations according to Fleeman (2001).

In simplified terms, a rocket launch consists of several steps. First, the rocket launches vertically upwards from the launch pad to gain altitude, keep the launch pad clear and also quickly overcome the lower atmospheric layers with high drag. The so-called gravity turn is then initiated: To achieve this, the flight path angle is deflected by a few degrees towards the horizon using control nozzles or engine gimbal (referred to as a pitchover manoeuvre or roll program). As a result, the rocket begins to lower the nose towards the horizon during the flight in accordance with the gravitational force in order to achieve more horizontal acceleration. During a rocket launch, an attempt is made to keep the angle of attack as small as possible. This means that there is negligible lift. In practice, the gimbal of the engine counteracts lateral forces and thus controls the trajectory. The magnitude of the deflection and the altitude of the pitchover manoeuvre can be used to optimize launch vehicle trajectories.

2.5 Methods to calculate emissions

To derive the species and mass of emissions, different approaches for calculating rocket emissions are summarized in Tab. 2 and are briefly discussed below. To address the uncertainties, we use the terms "very low, low, medium, high, very high" to define levels of confidence according to the IPCC reports Mastrandrea et al. (2010). The stated uncertainty levels are based on expert judgment.

https://doi.org/10.5194/egusphere-2026-3050
Preprint. Discussion started: 30 June 2026

Table 2. Overview of methods for emission index calculation. The consideration of different aspects and parameters is shown as well as an estimate of calculation effort by the authors and confidence level. The literature uses fixed or altitude-dependent emission indices. LEAT has implemented those but also provides a one-dimensional chemical equilibrium emission calculation representing a balance between computational effort and consideration of engine- and altitude-specific impacts on emissions.

Methodology	**Stoichiometric**	**Fixed**	**Altitude dependent**	**Chemical equilibrium 1D**	**Complex Numerical Simulation 2D/3D**	**Measurement**
Main emission	X	X	X	X	X	(X)
Minor emission	-	X	X	X	X	X
Engine-dependent	-	-	-	X	X	X
Altitude-dependent	-	-	X	X	X	(X)
Time- & location-dependent	-	-	-	X	X	(X)
Calculation effort	low	low	low	medium	high	low
Confidence level	very low	very low	very low - low	low - medium	low - medium	high - very high

2.5.1 Stoichiometric calculation

The simplest way to calculate emissions is the assumption of complete and stoichiometric combustion of propellants. This represents the maximum possible mass fractions of the main emission species for each propellant but does not take into account partial combustion and minor species. The equations for stoichiometric combustion are given in the supplementary material Sect. S1.1. Stoichiometric combustion does not occur in practice within engines because they are operated with an excess of fuel. Also for post-combustion, the interaction with the atmosphere depends on the ambient conditions (like available oxygen) changing with altitude and is therefore not stoichiometric.

2.5.2 Fixed emission index

Used in most recent publications, an engine-dependent fixed value for some emission species is used that is multiplied by the mass flow for calculating the emission. The approach which was used by Ross et al. (2010); Ross and Sheaffer (2014); Larson et al. (2017); Ryan et al. (2022); Pradon et al. (2023); Brown et al. (2024) is used for some minor emission species but does not account for variations in emissions with altitude or engine type.

2.5.3 Altitude-dependent emission index

James et al. (2021) provided a methodology which was used by Barker et al. (2024) to calculate altitude-dependent emission indices. This approach is divided into primary emissions (engine-specific) and derived secondary emissions dependent on

https://doi.org/10.5194/egusphere-2026-3050
Preprint. Discussion started: 30 June 2026

altitude. It is partly based on measurement data, partly on chemical simulations and takes into account main as well as minor emission. Post-combustion efficiency is considered by adjusting the emission index with altitude.

2.5.4 Chemical equilibrium 1D

One approach that accounts for both engine specifics and post-combustion in the environment, is to assume an equilibrium calculation, which allows for the calculation of more complex chemical reactions than the simpler approaches shown before. The chemical equilibrium calculation allows the consideration of engine-specific parameters like the oxidizer-to-fuel (or propellant component) mass ratio, nozzle expansion ratio for calculating the exhaust. If an implementation of the post-combustion is also conducted, the time- and location-dependent parameters like the atmospheric density and composition can also be taken into account. By using equilibrium reactions, more complex reactions of carbon, nitrogen and hydrogen compounds as well as the formation of thermal nitrogen oxides can be analysed. The computational effort is higher compared to the fixed or altitude-dependent values, but is still in the range of seconds on a laptop.

2.5.5 Complex numerical simulation 2D/3D

Since the real plume is turbulent and in reality, chemical processes neither occur in a perfectly mixed combustion chamber nor in equilibrium, complex calculations are necessary for detailed calculations. Common calculation methods are refined CFD simulations with reaction models (Troyes et al., 2006; Koch et al., 2013; Bauer et al., 2013; Ecker et al., 2019; Gomberg and Stewart, 1976; Stewart and Gomberg, 1976; Leone and Turns, 1994) or large-eddy simulations (Paoli et al., 2020; Poubeau, 2015). However, these models have the disadvantage that they require significant effort to create the model and the calculation itself compared to the equilibrium calculation and are therefore not suitable for the rapid calculation of emissions for each point along the trajectory. Therefore this is outside the scope of this paper.

2.5.6 Measurement-based values

Engine specific measurements of rocket launch emissions would provide ideal data for constraining emission indices. However, measurements of emissions are currently only available for a few engines given in the supplementary Tab. S7. Measurements at different altitudes are necessary to characterize the interaction with the atmosphere. Ground base measurements at testing sites, airplane-based measurements are an option. However, the measurement of rocket launch emission is challenging, especially from the upper stratosphere and above.

3 Model description

The Launch Emission Assessment Tool (LEAT) calculates individual rocket launch-specific 4D (time, altitude, longitude, and latitude) emission distributions. Fig. 3 shows the general workflow of the tool. The tool is based on two main calculation steps which are explained in more detail below. The first one calculates the trajectory based on the given input for the launch. The second one calculates emissions based on the trajectory and one of three different options, either fixed emission indices, CEA

https://doi.org/10.5194/egusphere-2026-3050
Preprint. Discussion started: 30 June 2026

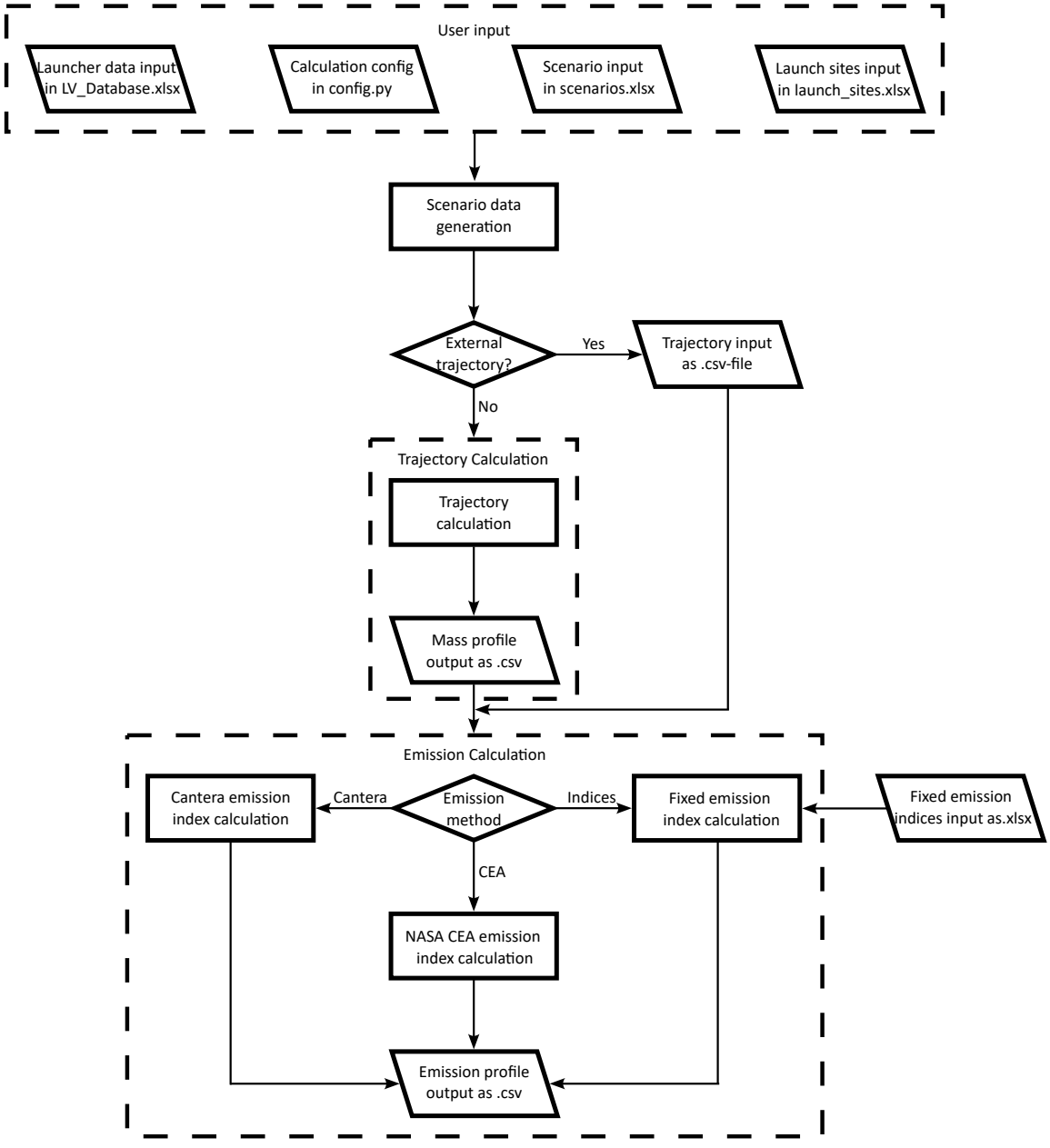

Figure 3. Schematic overview of the workflow in LEAT. Rectangles represent programmes, trapezoids represent inputs/outputs, and diamonds represent decisions. The dotted lines separate the individual steps: user input, trajectory calculation, and emission calculation. Both calculations can be executed independently of each other. User inputs for the rocket, launch scenario, and launch site information are provided as .xlsx files, the calculation is configured via parameters in config.py. A list of parameters is given in the supplementary material Sect. S4. The trajectory calculation determines the mass profile based on user input. Emission index calculation can be performed using emission indices, NASA CEA as well as Cantera (for liquid engines). The emission profile is the final output of the tool. Further explanations of the calculation logic are provided in Figs. 4 and S2 (Supplementary Material) and the text.

https://doi.org/10.5194/egusphere-2026-3050
Preprint. Discussion started: 30 June 2026

or Cantera. Each launch represents a "scenario" which is individually calculated by the tool. First, the input data are loaded and and stored in data frames. If the user chooses to calculate a trajectory, this is done using an ordinary differential equation (ODE) solver. Users can also provide their own trajectories for emission calculations. In the next step, the emissions are calculated. Either by using predefined fixed emission indices which are provided as input or by individually calculating the exhaust and emissions with CEA or Cantera for each altitude or time step in the trajectory data. The output corresponds to the trajectory file, the total emissions and the mass of individual emission species per altitude or time step. The output is provided in .csv format which can then be further processed into NetCDF or other data formats. In the following, the underlying models and assumptions are discussed for the trajectory and emission calculation.

3.1 User inputs

The tool requires inputs on the launch vehicle such as geometry, dry and propellant mass and information on thrust, burning time and propellant component mass ratio as well as the engine for each stage. These are provided in LV_Database.xlsx. Furthermore, the coordinates and altitude of the launch sites are stored in the launch_sites.xlsx. Based on this information, the scenario (representing an individual launch) is defined within the scenarios.xlsx. Here the launch date, inclination (converted by the program to the launch azimuth) and payload mass is added as well as the parameters on gravity turn and thrust reduction during ascend. The configuration of the calculation is defined in the config.py file which contains all the relevant parameters and file paths. A list of the required data and parameters is given in the supplementary material Sect. S3.

3.2 Trajectory calculation

Fig. S2 in the supplementary material illustrates the logic of the trajectory calculation code. The rocket launches from the given launch pad defined in the scenario and its trajectory is then calculated by solving the differential equations 2-5.

For the input, the user must define the parameters described in the Supplementary Material (Sect. S3). With the given initial values such as launch date, launch location and launch vehicle, the launch is divided into different phases. Each phase represents the operation of one stage or one stage with boosters operating simultaneously. Therefore, the launch of the Ariane 6 with a core stage, upper stage and additional boosters has three phases. The first phase considers the parallel burning of the core stage and booster stages. During the second phase, after booster separation, only the core stage is active. The third phase represents the burning of the upper stage. For coasting phases or stage separations, an intermediate "phase" without thrust can be defined within the tool (see the Falcon 9 case study additional input files).

LEAT calculates the trajectories using atmospheric density and pressure from the NRLMSIS model (Emmert et al., 2021) via its Python interface. The drag is calculated using the equations from Fleeman (2001), while thrust is calculated altitude-dependent by the following scheme:

$$F(h(p)) = F_{\mathrm{sl}} + (F_{\mathrm{vac}} - F_{\mathrm{sl}})(1 - p_{\mathrm{a}}/p_0) \tag{6}$$

where h is the altitude, F_{sl} is the thrust at sea level, F_{vac} is the thrust in vacuum, p_{a} is the current ambient pressure and p_0 represents the sea level pressure. The thrust can be reduced within a specified altitude range by multiplying the thrust reduction

https://doi.org/10.5194/egusphere-2026-3050
Preprint. Discussion started: 30 June 2026

factor from the user's input to take into account the thrust reduction during passage through the point of maximum dynamic pressure (typically called max-Q) to reduce aerodynamic loads. The mass flow of the exhaust is calculated based on the given propellant mass of the stage and the burning time assuming a constant mass flow. It is adjusted during the thrust reduction phase. The trajectory calculation is then conducted by an ODE solver for each time step defined by the user (default: 0.1 s). Optionally, the output can also be compressed with respect to altitude or time to speed up the subsequent step-wise emission calculation. The output from this calculation is a trajectory file that contains the relevant input for the emission calculation, namely the time since launch, altitude, date, longitude, latitude, velocity, total mass of exhaust, active phases and time intervals for the defined altitude or time steps. A more detailed trajectory file with all trajectory parameters calculated (e.g. downrange, γ, F) is also generated.

Table 3. Overview of the three emission index calculation approaches implemented within LEAT. The table shows the thermodynamic consideration of the steps within and outside a rocket engine as well as different options for each approach. Emission indices come with either stoichiometric, fixed or altitude-dependent datasets. All available literature values are implemented. CEA offers with the rocket problem calculation an equilibrium or frozen (from a certain point onward). Cantera is implemented only for liquid engines and represents an equilibrium calculation. hp = constant enthalpy and pressure, sp = constant entropy and pressure

Model	**Emission indices**	**CEA**	**Cantera**
Calculation approach	Fixed values	Two Step Equilibrium calculation	Four Step Equilibrium calculation
Gas Generator	N/A	Rocket problem	N/A
Combustion Chamber	N/A	Rocket problem (hp)	hp
Throat	N/A	Rocket problem (sp)	sp
Nozzle	N/A	Rocket problem (sp)	sp
Post-combustion	Fixed	Combustion hp	hp
Options	Stoichiometric, fixed or altitude-dependent factors from literature	Equilibrium or frozen at certain point (e.g. throat)	N/A

3.3 Emission calculation

From the calculation options described in Sect. 2.5 the following options are available in LEAT: (i) emission indices (fixed or altitude-dependent), (ii) CEA (Gordon and McBride, 1994) calculation using the equilibrium or frozen method and (iii) Cantera (Goodwin et al., 2024). Due to the high computational cost of CFD calculations and the limited availability of measurement data these other calculation options were neglected. The workflow for the emission calculation within LEAT is shown in Fig. 4. Following this schematic, we describe the individual steps that are performed within LEAT in more detail.

https://doi.org/10.5194/egusphere-2026-3050
Preprint. Discussion started: 30 June 2026

3.3.1 Emission indices method

The emission indices method uses pre-defined emission indices, either fixed or altitude-depended and represents the final emissions after interaction with the atmosphere. The factors depend only on the chosen propellant defined in the *LV_Database* input file and on altitude. To use this method the *use_emission_factors* value must be set to *True* in the *config.py* file. Emission indices are defined within the *emission_indices.xlsx* input file. Multiple predefined options are available which are selected with the *emission_factor_method* parameter in the *config.py*:

- **stoichiometric** assuming a complete combustion of fuel within the atmosphere, independent of altitude by setting *emission_factor_method='stoichiometric'*
- **LEAT** example values from tool results in 5 km bins by setting *emission_factor_method='LEAT'*
- **Literature** values from publications containing altitude-depended values from James et al. (2021); Barker et al. (2024) and fixed values from Ross et al. (2010); Ross and Sheaffer (2014); Larson et al. (2017); Ryan et al. (2022); Pradon et al. (2023); Brown et al. (2024) by setting *emission_factor_method='name of literature source'*
- **user-defined values** by adding them for specific propellants and altitude intervals in the *emission_indices.xlsx* input file and naming them in the *method* column, setting *emission_factor_method='chosen name of the user-defined method'*

3.3.2 CEA method

With an additional free license for the software "Chemical Equilibrium with Applications" (CEA) the user of LEAT can calculate the engine emissions considering different options. This is implemented in the code as the function *run_nasa_cea*. CEA enables the calculation of chemical equilibrium states. The thermodynamic assumptions are given by the developers Gordon and McBride (1994): *"one-dimensional form of the continuity, energy, and momentum equations; zero velocity at the combustion chamber inlet; complete combustion; adiabatic combustion; isentropic expansion in the nozzle; homogeneous mixing; ideal-gas law; and zero temperature lags and zero velocity lags between condensed and gaseous species."*. The program iteratively adjusts the thermodynamic state variables so that the free energy is minimized. With CEA, the user can calculate the engine exhaust with a *rocket problem* and the final emissions using an *hp problem*. The program uses different thermodynamic assumptions for the various combustion phases within the rocket engine and for the post-combustion. The *rocket problem* is used for calculating the combustion chamber, the throat and attached nozzle. CEA operates under the assumption of an assigned enthalpy h and pressure p within the chamber, for the throat and nozzle exit fixed entropy s (isentropic expansion) and assigned exit pressure p. Post-combustion is calculated using fixed enthalpy h and assigned pressure p. As an input, the propellant defined in *LV_Database.xlsx*, the oxidizer-to-fuel ratio $m_{\mathrm{ox}}/m_{\mathrm{fu}}$ or propellant components mass ratio in the case of a solid propellant, the combustion chamber pressure p_{c} and the nozzle expansion ratio $a_{\mathrm{e}}/a_{\mathrm{t}}$ defined within the *LV_Database - Engine* sheet are required.

https://doi.org/10.5194/egusphere-2026-3050
Preprint. Discussion started: 30 June 2026

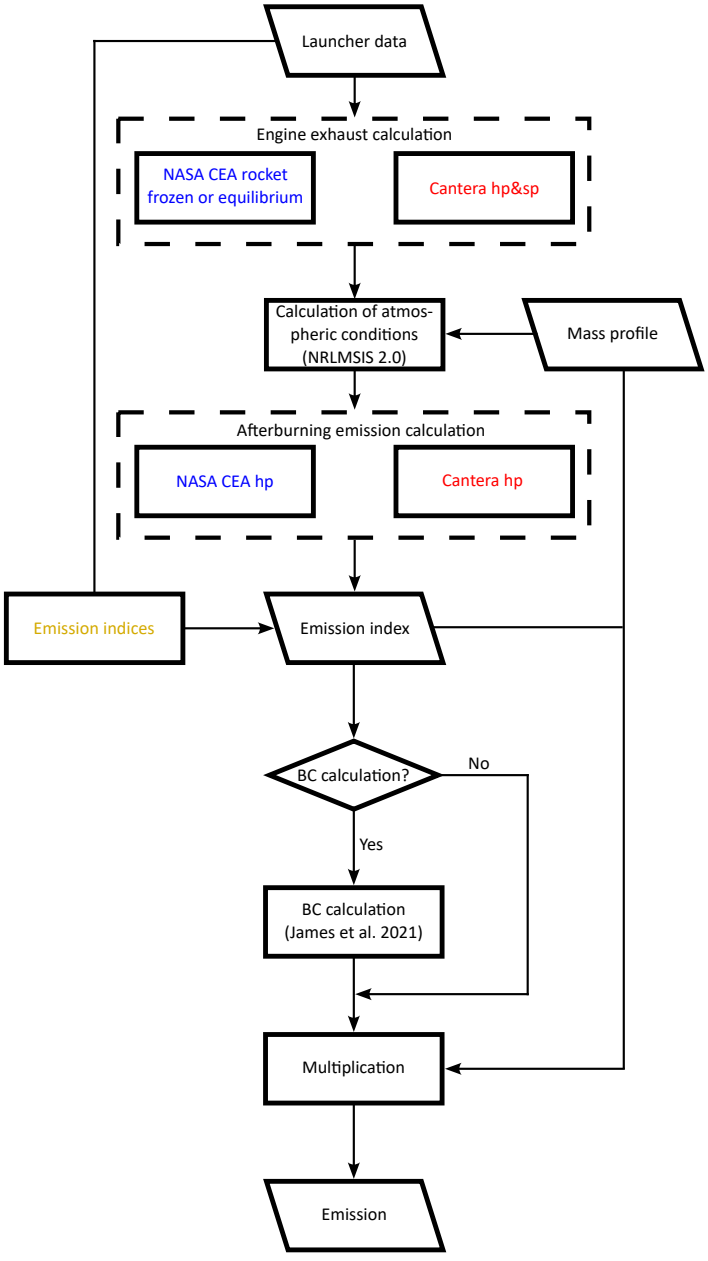

Figure 4. Schematic overview of the emission calculation logic. Rectangles represent programmes, trapezoids represent inputs or outputs, and diamonds represent decisions. Dashed lines represent the two-step calculation first at the engine exhaust and second for the final emission calculations. Different calculation approaches are available based on CEA (blue), Cantera (red) and emission indices (orange). The engine exhaust calculation is executed once per staging phase, whereas the post-combustion emission calculation is executed for each altitude step. See text for details.

https://doi.org/10.5194/egusphere-2026-3050
Preprint. Discussion started: 30 June 2026

CEA assumes either *equilibrium* or *frozen* combustion. For *equilibrium*, all reactions happen until the chemical equilibrium is reached. For the *frozen* option, the user can decide at which level the reactions freeze. From that point on only expansion happens. The point can be chosen to be after the combustion chamber, throat or nozzle. The throat is the default setting as the reactions are assumed to freeze within the nozzle. The exit pressure p_{e}, temperature T_{e} and species mass fraction (=exhaust composition) EX_{e} is then saved. If the user wants to calculate a separate gas generator which emits directly into the atmosphere this can also be done by a *rocket problem* via selecting the *GG* (gas generator) engine cycle within the *LV_Database - Engine* sheet. If this is the case the exhaust from the engine is mixed according to the mass flow fraction of the open cycle $\dot{m}_{\mathrm{oc}}$.

Using the data from the trajectory calculated or provided for altitude h, time, latitude, and longitude, the ambient air state variables pressure p_{a}, temperature T_{a} and density ρ_{a} and the local and time-dependent composition of the ambient air can then be derived using the NRLMSIS atmospheric model (Emmert et al., 2021). For calculating the mixing with the atmosphere, a control volume starting at the nozzle exit is assumed (see also Fig. S3 in the supplementary material). The mass flow at the intake of the control volume m_{in} is defined by the mass flow from the engine m_{exh} plus the mass flow from the surrounding air m_{air}. The latter is calculated using the post-combustion uncertainty mixture factor x_{ab} which is multiplied with the rocket reference area A_{r}, representing the effective intake area the ambient air flows through. The resulting mixture air mass flow m_{air} is dependent on rocket size, the relative velocity v_{air}, assumed equal to the rocket velocity (assuming no winds) and the local air density ρ_{air}.

$$\dot{m}_{\mathrm{in}} = \dot{m}_{\mathrm{air}} + \dot{m}_{\mathrm{exh}} \tag{7}$$

$$= A_{\mathrm{air}} v_{\mathrm{air}} \rho_{\mathrm{air}} + \dot{m}_{\mathrm{exh}} \tag{8}$$

$$= A_{\mathrm{r}}(x_{\mathrm{ab}} - 1) v_{\mathrm{air}} \rho_{\mathrm{air}} + \dot{m}_{\mathrm{exh}} \tag{9}$$

$$\tag{10}$$

The final air-to-exhaust mixing ratio ROF_{ab} is then calculated with the mass flow of the engine m_{exh} and m_{air}.

$$ROF_{\mathrm{ab}} = \frac{\dot{m}_{\mathrm{air}}}{\dot{m}_{\mathrm{exh}}} \tag{11}$$

Within this control volume, we assume the conservation of mass as well as an (idealistic) adiabatic reaction without heat exchange over the boundaries of the control volume. The emission index *EI*, defined as the mass fraction of emitted species w_{emi} can be calculated from the results of the post-combustion calculation w_{ab} by subtracting the original air species mass fractions w_{air}.

$$EI_{\mathrm{emi}} = w_{\mathrm{emi}} = (w_{\mathrm{ab}}(ROF_{\mathrm{ab}} + 1)) - (w_{\mathrm{air}} ROF_{\mathrm{ab}}) \tag{12}$$

yielding the emissions as

$$\dot{m}_{\mathrm{emi}} = EI_{\mathrm{emi}} \dot{m}_{\mathrm{exh}}. \tag{13}$$

https://doi.org/10.5194/egusphere-2026-3050
Preprint. Discussion started: 30 June 2026

3.3.3 Cantera method

In addition to CEA, an alternative calculation can be performed using Cantera (Goodwin et al., 2024). Unlike CEA, Cantera can be integrated as an open-source Python library with an open-source license. This allows the tool to be used for liquid propellants without a CEA license. The workflow within LEAT is the same as when CEA is used (see also Fig. S4).

For the rocket emissions the Python implementation of a thermodynamic combustion logic developed by Niemeyer (2026) was used. An additional *.yaml* input file was generated based on the CEA thermodynamic database *thermo.lib*. As for CEA, a two-step calculation approach is used where first the exhaust is calculated at the nozzle exit. Within the Cantera integration, the combustion chamber is calculated with a *hp* equilibrium solver, the throat and nozzle with a *sp* equilibrium solver, consistent with the CEA assumptions. In a second step, the post-combustion is integrated as described in the section above. The calculation of the post-combustion is limited to an air-to-exhaust ratio of 0.01. Below that value, the equilibrium solver fails in most cases. As the exhaust mass flow is then the dominant flow it is treated as the emission. It is important to mention that for the post-combustion the specific heat capacity definition c_p used in Cantera assumes frozen composition while the one from CEA is adapted instantaneously to the new equilibrium (Niemeyer, 2026).

3.3.4 Black carbon emissions

Although the formation of black carbon (also known as soot) particles in rocket engines is frequently discussed in the literature, little research on the atmospheric effects of rocket launches has been carried out to date (Ross et al., 2010; Ross and Sheaffer, 2014; Maloney et al., 2022). There are a few publications on the formation of black carbon in rocket engines (Nickerson and Johnson, 1992; Sheaffer, 2021; Stryjewski, 2001; Plastinin et al., 2005; James et al., 2021). The values given in the literature are based on assumptions (same BC for different propellants, derivations from other engines; James et al., 2021) except for a few measurements of Athena II (Rudman, 1994; Cziczo et al., 2002; Danilin et al., 2003; Popp et al., 2002; Schmid et al., 2003), a LOX/RP-1 rocket engine, the F-1 engine (Herget, 1965) and the Space Shuttle SRM (Cziczo et al., 2002). Since the effects of black carbon from rocket launches are expected to have a major influence on climate and ozone (Ross et al., 2010; Maloney et al., 2022), it is particularly important to address the uncertainty in the calculation. Currently, there are mainly altitude-independent emission indices in the literature. However, it can be expected that the black carbon particles in the denser atmospheric layers continue to burn, which is also indicated by the orange glow of exhaust plumes. As the rocket climbs higher, two phenomena come into play. Firstly, there is less atmospheric oxygen available for oxidizing the black carbon particles in the post-combustion process, and secondly, the plume fans out further and further, causing the temperature to fall faster. It is therefore expected that post-combustion of black carbon only takes place in the sufficiently dense parts of the atmosphere. A model to take these processes into account was developed by James et al. (2021), implemented within the tool when selecting *calculate_black_carbon*, based on measurement and simulation data from Simmons (2000), Alexeenko et al. (2002) and Plastinin et al. (2005). This reads:

$$EI_f(\mathrm{BC}) = EI_p(\mathrm{BC}) \max\left(0.04, \min\left[1, 0.04\, e^{(0.12/\mathrm{km})(h-15\,\mathrm{km})}\right]\right) \tag{14}$$

https://doi.org/10.5194/egusphere-2026-3050
Preprint. Discussion started: 30 June 2026

with $EI_p(BC)$ = 25 g/kg for LOX/RP-1, N_2O_4/UDMH, solid and N_2O_4/HTPB as well as 5 g/kg for LOX/CH_4 (James et al., 2021). It is noteworthy that those numbers are, except for LOX/RP-1 based either on assumptions by James et al. (2021) or on additional literature (Simmons, 2000; Plastinin et al., 2005; Alexeenko et al., 2002). In addition to the mass of emitted black carbon particles, the particle size distribution is also relevant as it influences the residence time in the atmosphere and thus the time to interact with radiation and affect ozone chemistry. A model by Simmons (2000), which is based on the measurements for the Athena II rocket, results in a normal distribution around the mean value of 40 nm. It should be noted that the size distribution refers to individual particles. It can be assumed that agglomeration in the exhaust jet also produces non-isometric particles with larger diameters, which are removed from the atmosphere more quickly. However, there is a lack of measurements and reliable models to describe these mechanisms precisely.

4 Results and evaluation

In this section, case studies for the Falcon , Starship, and Ariane 6 launch vehicles are presented. First, trajectory results calculated with LEAT are compared with data from actual launches. Furthermore, for the three case studies, we show the mass profiles, exhaust compositions for the different calculation approaches as well as a preliminary uncertainty analysis of the final emissions. A more detailed analysis of uncertainties and the impact of input parameter variations such as gravity-turn altitude will be part of the companion paper.

4.1 Case study selection

To motivate the selection of the case studies, all rocket launches in 2024 are analysed in more detail. In Fig. 5, the number of successful orbital launches per rocket type in 2024 are shown in the outer ring based on McDowell (2026). Over half of all launches were carried out by the Falcon (RP1/LOX). Electron (also RP-1/LOX) follows in second place with 10% of launches. This is followed by Soyuz-2-1A (RP1/LOX) and the Chinese Long March 2D, 3B, and 2C (all UDMH/NTO) and Soyuz-2-1B (RP1/LOX). Launchers with fewer than 2 launches were grouped together in “Others”. The inner ring shows the proportional distribution of consumed propellant mass in 2024 across all stages. RP1/LOX is the most widely used propellant with over three quarters. This is followed by UDMH/NTO with 9.4% and CH_4/LOX with 8.4%. It should be noted that the latter proportion is by 99% driven by the four test flights of the Starship conducted in 2024.

Against this background, the results from LEAT are compared with launch data, which is available through video streams. The video data was extracted with a modified code based on the work of Billington (2023). We select three case studies based on the propellant usage in 2024 and expectations for the future:

1. A flight of the Falcon (RP-1/LOX) 58th Starlink Group 4-23 mission from Cape Canaveral representing the most widely used propellant and launch vehicle in 2024 was selected. Starlink is currently the most launched payload into orbit. Therefore, in the following the 58th Starlink Group 4-23 mission from LC-40 Cape Canaveral at the 28th August 2022, 03:41 UTC is analysed as a case study. The mission successfully deployed 54 Starlink-Satellites into an orbit of 540 km with an inclination of 53.2°. The video data is available from SpaceX (2022).

https://doi.org/10.5194/egusphere-2026-3050
Preprint. Discussion started: 30 June 2026

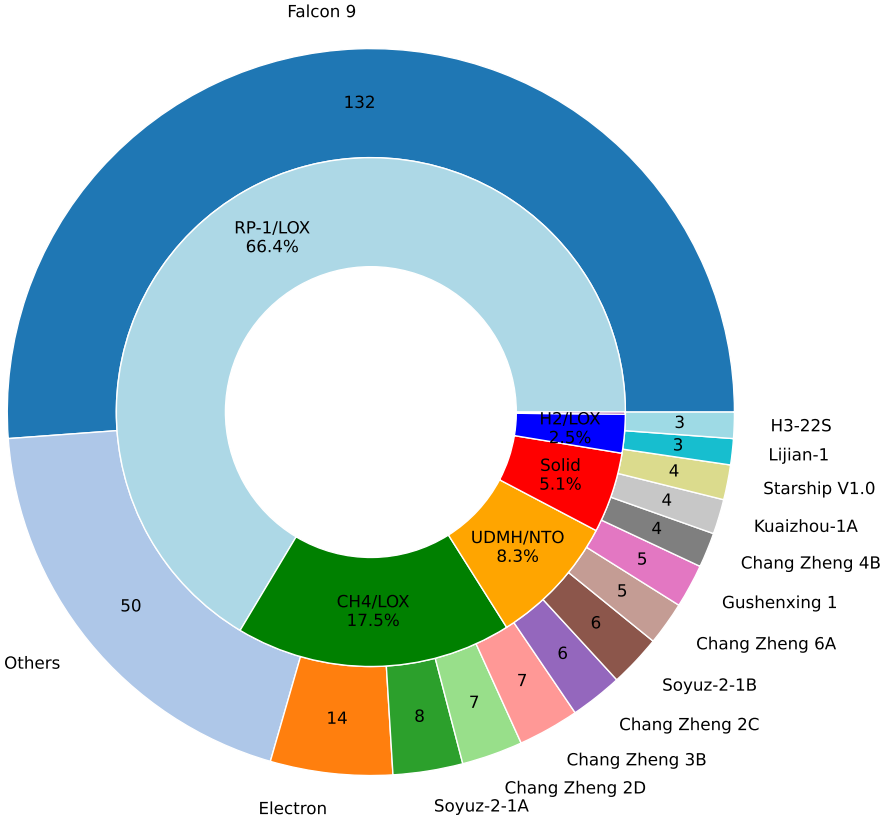

Figure 5. Share of launch vehicle types (outer circle) and propellant combination (inner circle) of successful orbital launches 2024 based on McDowell (2026). Launchers with fewer than 2 launches were grouped together in "Others". The split up of propellant consumption was calculated based on all stages. Other propellants are 0.1%. Falcon was dominating the launcher market with more than half of the launches. Kerosene/LOX was the most used propellant in 2024 followed by UDMH/NTO and CH4/LOX (mainly driven by Starship test flights).

2. The 8th test flight of the Starship (CH_4/LOX) was chosen to represent the expected future dominant launch vehicle in terms of emissions. Starship is currently under development and has conducted several test flights. One flight burns ten times the propellant mass of one Falcon launch and therefore represents roughly an order of magnitude higher emissions. We have chosen IFT 8 with the Starship V2 as it was the last flight with full trajectory data within the video stream. The flight was launched on 6 March 2025 at 23:30:31 UTC and ended with the explosion of the upper stage and a successful catch of the booster stage. The video data is available from SpaceX (2025).

https://doi.org/10.5194/egusphere-2026-3050
Preprint. Discussion started: 30 June 2026

3. Finally, the tool's capability of calculating trajectories and emissions from VA263 of Ariane 6 (H_2/LOX + Solid) is evaluated. This launch vehicle represents an interesting case study for the tool with the combination of solid booster and a cryogenic core stage. Ariane 62 first commercial flight, VA263 launched the CSO-3 satellite into a Sun-synchronous orbit at 800 km altitude with an inclination of 98°. It launched at 6th March 2025 at 16:24 UTC. The video data are available from Arianespace (2025).

4.2 Trajectory evaluation and mass profile analysis

For the calculation of the trajectory the gravity-turn angle was varied between 0.5° and 3.0° and the gravity-turn altitude was varied between 10 m and 500 m altitude. With this, the calculated flight paths were adjusted to the real flight data. A detailed list of selected parameters can be found in the supplementary material Tab. S8. The scenario file can be found in the additional files.

Figure 6 shows a comparison of trajectory data extracted from the video stream and the trajectory data calculated with LEAT. The orange line shows data from the core stages, the red line shows data from the upper stage (where applicable) both derived from the video stream. The blue shaded area shows the spread of the trajectories calculated with LEAT for different gravity turn angles and altitudes. The blue line represents the trajectory which represents the best estimate and is taken for emission calculation in the following (see Sect. 4.4).

The best estimate for the Falcon launch is shown in Fig. 6a. It was reached with an initiation altitude of gravity turn between 140 and 190 m and a $\Delta\gamma$ of 1.5. It can be seen, that for our best estimate there is overall very good agreement of the altitude vs. time profile with the live stream data. The resulting mass profile of the launch is given in Fig. 6b. The largest share of propellant is emitted within the first kilometres (about 1/3 of total propellant within the first 15 km, 1/2 within the first 31.5 km). In total 334,795 kg of propellants are exhausted up to 100 km (73% of total propellant). At 5-10 km the thrust reduction during passage through max-Q (point of maximum dynamic pressure) is represented with a reduction in emissions at this altitude. At 67 km the stage separation takes place where the main engine is cut off and the second engine takes a few seconds to start at about 77 km. This creates a gap in the mass profile (65 km-75 km). After that the upper stage engine runs with 1/9 of the mass flow of the core stage. The Starship calculation shows a good agreement between LEAT calculation and actual flight data in the altitudes between 0 and 40 km. The LEAT simulation was obtained with values for the altitude of the gravity turn between 50 m - 100 m with a $\Delta\gamma$ of 0.5. In this altitude region the deviations are in the order of the Falcon case. Above 40 km the deviations increase steadily. LEAT calculates that the rocket climbs too rapidly. In reality, Starship takes longer to build up vertical velocity. In LEAT, a constant maximum thrust profile is assumed except for the launch phase and thrust reduction to minimize aerodynamic pressure. In reality, two aspects play a role. On the one hand, the IFT-8 flew a suborbital trajectory, which does not require full thrust. On the other hand, active control of the flight angle could also be carried out to facilitate the return of the core stage to the launch platform. Therefore, the calculations deviate when assuming an orbital flight profile with a full thrust curve. It would be possible to consider lower thrust or active flight path angle control via implementing this in the code.

https://doi.org/10.5194/egusphere-2026-3050
Preprint. Discussion started: 30 June 2026

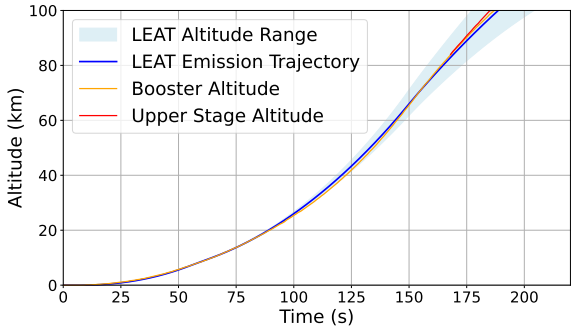

(a) Falcon Starlink

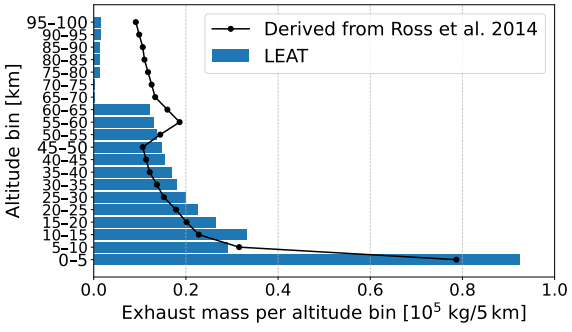

(b) Mass profile

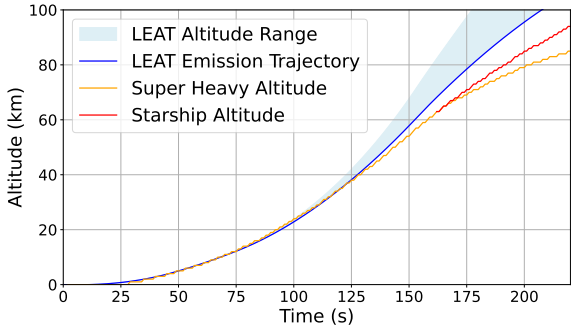

(c) Starship IFT-8

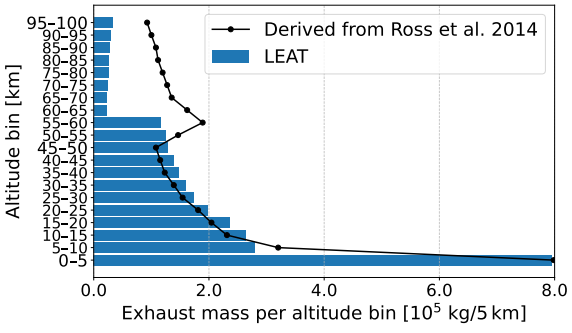

(d) Mass profile

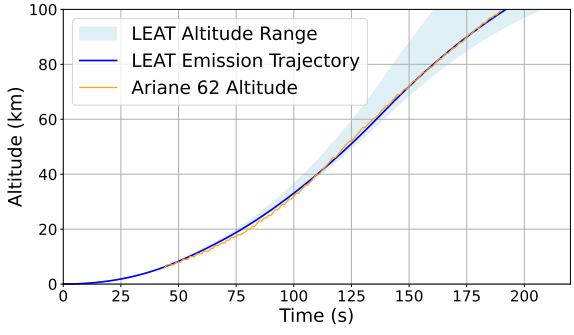

(e) Ariane 62

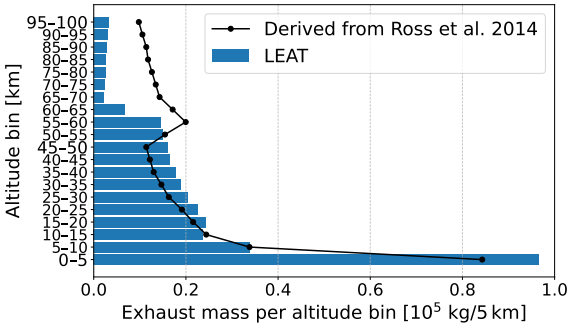

(f) Mass profile

Figure 6. a) Trajectory and b) mass profile of Falcon 9 Starlink launch on 28 August 2022, Starship IFT-8 launch on March 6, 2025, 23:30:31 UTC and Ariane 62 VA263 launch on 6 March 2025 at 16:24 UTC. The trajectory profile shows flight data extracted from video streams (orange and red lines for the core and upper stages) and LEAT-calculated trajectories with varied parameters (blue line and blue shading). The blue shading represents different LEAT calculations with variations in gravity-turn parameters. The blue line shows the best estimate and is chosen for the emission calculation. The orange and red lines represent flight data extracted from video stream for core and upper stage, respectively. The mass profile shows the mass distribution as a function of altitude. The gaps at higher altitudes represent the staging phase. A mass profile derived from Ross and Sheaffer (2014) is shown for comparison by multiplying the mass fraction with the total launch vehicle propellant mass.

https://doi.org/10.5194/egusphere-2026-3050
Preprint. Discussion started: 30 June 2026

Super Heavy, the core stage from Starship accelerates back toward the launch tower after separation which is not represented in the LEAT trajectory calculations and explains the differences compared to the actual flight path data (orange line). It is planned to include the return of stages within a later version of LEAT. Fig. 6d shows the mass profile of the Starship launch. In total 2,976,595 kg of propellants are exhausted below 100 km (64.2% of total propellant). One third of the total propellant is exhausted within the first 19.5 km, 1/2 within the first 42.5 km. Here, the thrust reduction can again be observed between 5-10 km altitude, however the exhaust mass does not fall below that of the preceding altitude bin. Hot staging during flight also has an impact on the mass flow profile, since there is no gap in the exhaust during stage separation. In Fig. 6e the trajectory of the Ariane 62 flight calculated by the tool is compared to the flight data from the video stream. The transmission of trajectory data from the video stream started at an altitude of 6 km. The differences between the actual flight data and the best estimate from LEAT reach at most 2-3 km in altitude at an altitude of 20 km and therefore show good agreement with the simulated data. The mass profile of the Ariane 62 launch shown in Fig. 6f is strongly impacted by the two solid boosters. As they operate with nearly seven times higher mass flow compared to the core engine, the separation from the core stage at 62 km results in a significant drop. Furthermore, the Ariane 6 core stage extends beyond 100 km, therefore the upper stage mass profile cannot be seen here. In total 346,197 kg of propellant is exhausted (70.7% of total propellant). One third of the total propellant is exhausted within the first 17 km, 1/2 within the first 36.5 km. The decline between 10 and 15 km represents a throttle-down phase.

4.3 Exhaust evaluation

For the exhaust calculation at nozzle exit level the engine and propellant parameters for the Falcon Merlin engine (LOX/RP-1) and the Ariane 6 P120 solid rocket motor (HTPB/Al/APN) were considered (Raptor and Vulcain figures can be found in the supplementary material Sect. S2.3). An additional gas generator burning in parallel to the main engine was taken into account for the Falcon Merlin in the CEA case. The parameters used can be found in the supplementary material Tab. S9 and within the engine worksheet in the LV-Database-file in the additional files. Fig. 7a shows the exhaust at nozzle exit level for the Falcon core stage Merlin engine. The largest share of exhaust with CEA Equilibrium is CO at 36.1%, CO_2 at 34.0%, H_2O at 25.8%, BC, represented in CEA as C(cr) for crystalline carbon, at 1.8%, H_2 at 1.3%, and CH_4 at 1.0%. The values are slightly different for CEA Frozen, with CO at 42.0%, H_2O in second place with 26.0%, CO_2 at 24.9%, OH at 2.3%, BC also at 1.8%, H_2 at 1.1%, CH_4 also at 1.0%, and additionally O_2 at 0.6%, O at 0.2%, and H at 0.1%. All other emission species have a value of less than 0.01%. Without taking the gas generator into account, the values for CEA Equilibrium and Cantera are identical at CO 37.2%, CO_2 35.2%, H_2O 26.3%, and H_2 1.2%. CEA Frozen deviates from this with CO 43.3%, H_2O 26.6%, CO_2 25.7%, OH 2.4%, H_2 1.0%, O_2 0.6%, O 0.3%, H 0.1%. For the Ariane 62 booster engine the exhaust in Fig. 7b is shown. Al_2O_3 emissions account for the largest share at 35.9%. This is followed by CO at 22.6%, HCl at 21.3%, N_2 (8.3%), H_2O (7.1%), CO_2 (2.4%), H_2 (2.3%) and Cl at 0.1%. The values are identical for the equilibrium and frozen approaches. All other emissions are equal or below 0.01%, with more species present in equilibrium.

https://doi.org/10.5194/egusphere-2026-3050
Preprint. Discussion started: 30 June 2026

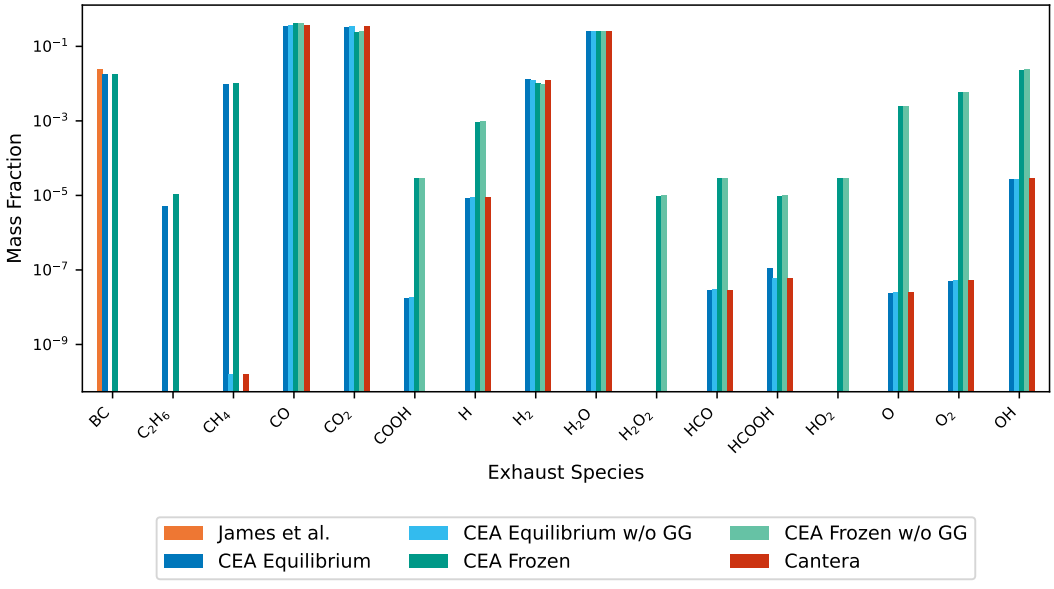

(a) Falcon 9 Merlin engine exhaust

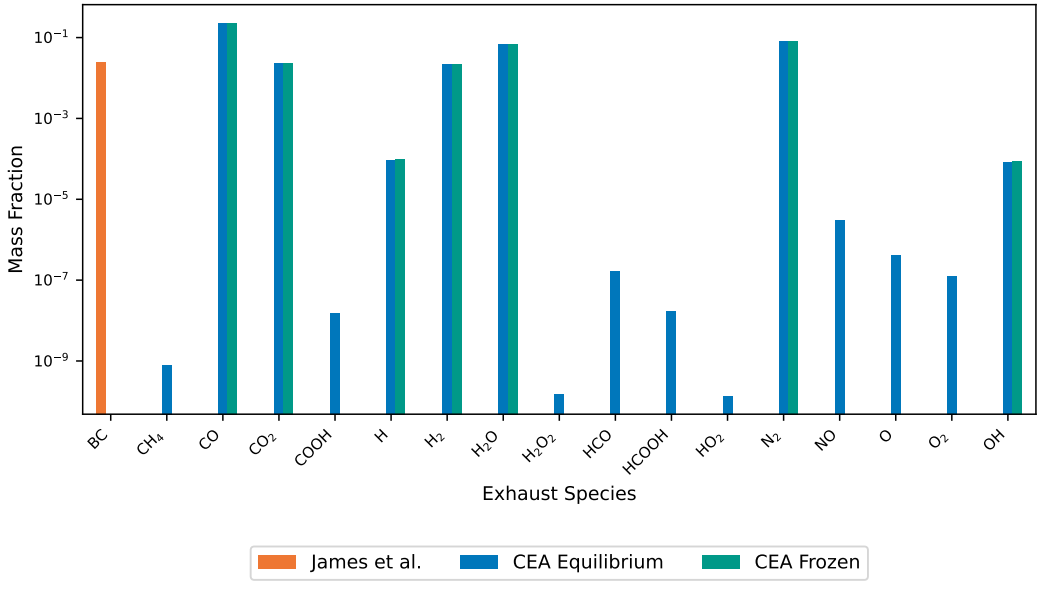

(b) Ariane 6 solid booster exhaust

Figure 7. Exhaust at nozzle exit of a) a Falcon Merlin engine and b) an Ariane 6 solid booster shown for the CEA equilibrium and frozen calculation approaches on a logarithmic scale. Species with a mass fraction less than 1^{-10} are not considered. Main species are CO, CO_2 and H_2O. An additional gas generator (GG) leads to additional BC, CH_4 and C_2H_6 within the exhaust. A greater variety of minor species can be seen for the frozen approach for liquid engines indicating unreacted O_2. CEA equilibrium and Cantera show consistent results. The BC estimate from James et al. (2021) is consistent with the calculation. For the solid engine, when considering frozen reactions from the nozzle exit onward, the equilibrium methodology shows more minor species.

https://doi.org/10.5194/egusphere-2026-3050
Preprint. Discussion started: 30 June 2026

4.4 Emission calculation method intercomparison

To assess the effect of post-combustion efficiency on our emission profiles, we investigate the impact of the in-mixing of ambient air within the hot plume on the post-combustion process, which is parametrized by the factor x_{ab} (see Sect. 3.3.2). For our calculations x_{ab} was varied between 1.2, 2, 4, and 8. A value of 1.2 corresponds to the minimum expected mass flow compared to launch vehicle cross-section and a value of 8 leads to full stoichiometric combustion below 15 km altitude. The impact of considering an equilibrium or frozen approach as well as the uncertainty factor on a global inventory level will be discussed in more detail in the second part of the paper. In the following, a selection of emission plots is shown with a focus on main similarities and differences for major and minor species. For the species CO_2, CO, H_2O, H_2, NO, OH, Al_2O_3, BC, Cl, Cl_2, HCl, representative examples of one of the three launches were selected. More emission species are emitted, but these are not as relevant either in terms of their quantity or in terms of their effects as discussed in the literature to date. The additional figures and a table containing all relevant species for each launch can be found in the supplementary material Sect. S1.6 and S2.4. For the CEA frozen and equilibrium approaches the post-combustion was run with a CEA *hp* problem. For the Cantera approach the post-combustion was calculated with a Cantera *hp* solution. The mass flow of surrounding air was calculated with the given x_{ab}. In Fig. 8a and Fig. 8b the emission profiles are shown for the gaseous species CO_2 and CO. Both figures are from the same Falcon launch and show the amount of the species emitted in kg/km. The drop in emissions at 7 to 10 km is the thrust reduction during ascend. Between 66 and 75 km there are no emissions as stage separation takes place. The coloured areas come from varying the post-combustion efficiency by adjusting the parameter x_{ab} between 1.2 (selected as a realistic minimum value) and 8 (leading to full stoichiometric combustion at lower atmospheric layers). The thick lines represent $x_{\mathrm{ab}} = 2$ for each calculation methodology. It should be noted that for the first 20 km the frozen and equilibrium approaches show nearly no CO emissions for $x_{\mathrm{ab}} = 8$ as enough atmospheric oxygen is present for CO to fully react to CO_2. This is also the uncertainty visible through the coloured areas for CO and CO_2 up to about 40 km, representing the altitude up to which noticeable post-combustion takes place. In total, up to 100 km between 105,625 and 244,830 kg of CO_2 are emitted according to CEA, 125,175 - 226,083 kg according to Cantera and 56,200 - 143,710 kg of CO are emitted according to CEA and 55,977 - 120,449 kg according to Cantera compared to 363,904 kg of CO_2 and 10,801 kg of CO with the emission index approach $\mathrm{EI}_{\mathrm{B24}}$.

Fig. 8c shows the nitric oxide profile of a Falcon launch. It can be seen that there are large differences for the different calculation approaches, which are more pronounced than for the other exhaust species. The Cantera approach has an order of magnitude higher NO emissions (6 - 12,770 kg) compared to the CEA approach (0.2 - 2,526 kg) but with a very large margin of uncertainty compared to 1,982 kg of NO_x with the emission index approach $\mathrm{EI}_{\mathrm{B24}}$. It is noteworthy that there are also NO_2 emissions in the order of a few kg per altitude for CEA and Cantera calculation approaches. Fig. 8d shows the OH emission profile from a Falcon launch. The highest OH emissions are obtained with Cantera (112 - 8,399 kg), while calculations using CEA (12 - 2,549 kg) only produce about 1/3-1/10 of the amount. The CEA emissions show various local maxima and minima over an altitude range from 15 km to 35 km while the Cantera emissions decrease constantly with altitude.

Fig. 9a shows the H_2O and H_2 emissions from a Starship launch. While the change in x_{ab} has only very little effect on H2O emissions (1,340,479 - 1,394,015 kg), for x_{ab} = 8 only very little H_2 is present at lower altitudes as enough atomic oxygen

https://doi.org/10.5194/egusphere-2026-3050
Preprint. Discussion started: 30 June 2026

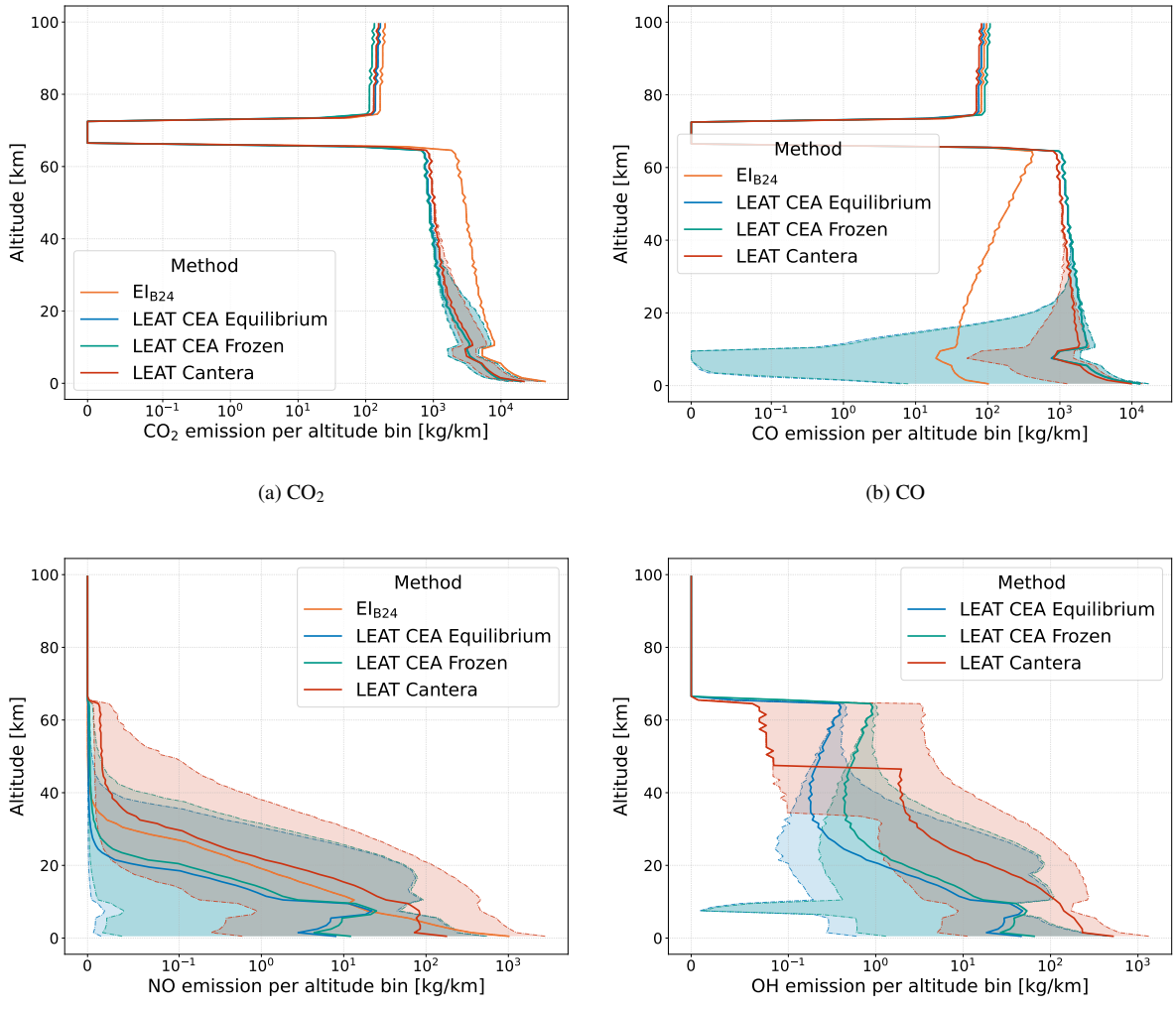

(a) CO_2 (b) CO

(c) NO (d) OH

Figure 8. Final emissions of the Falcon launch as a function of altitude shown for different calculation methodologies. Shaded areas represent x_{ab} = 1.2 - 8, lines represent x_{ab} = 2. The decline at lower altitudes represents thrust reduction. Gap at higher altitudes represents stage separation. CEA equilibrium (blue) and CEA frozen (green) approach are overlapping for CO_2 and CO. Cantera approach (red) leads to different results. CO_2 shows little variance in the change of the factor. CO is not formed for lower altitudes if enough atmospheric mass flow is considered. NO and OH emissions show a wide range of uncertainty with varying factor. Altitude-dependent emission indices derived from Barker et al. (2024) methodology (EI_{B24}, orange) show less CO formed, but higher NO for lower altitudes.

https://doi.org/10.5194/egusphere-2026-3050
Preprint. Discussion started: 30 June 2026

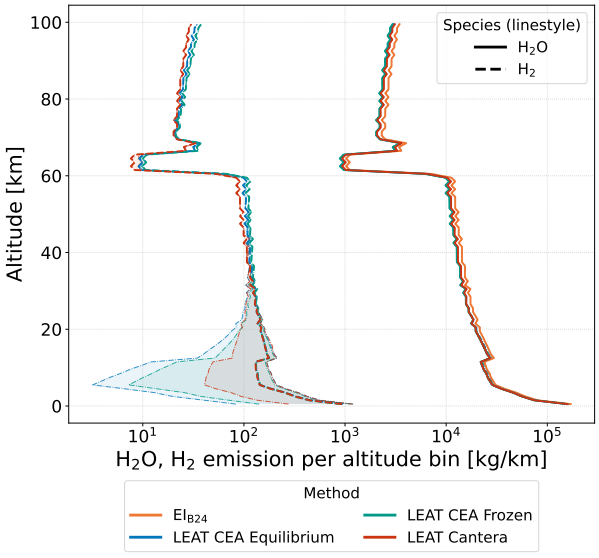

(a) H_2O

Figure 9. Final emissions of the Starship IFT-8 launch depending on altitude shown for different calculation methodologies. Areas represent x_{ab} = 1.2 - 8, lines represent x_{ab} = 2. Decline at lower altitude represents thrust reduction. Decline at higher altitudes represents hot stage separation. CEA equilibrium (blue), CEA frozen (green) and Cantera (red) approaches are overlapping for H_2O. H_2O shows no variability with changing factor. Formation of H_2 is not considered in literature.

for the reaction during post-combustion is present leading to a range from 5,847 - 11,372 kg. Comparing the emission index approach EI_{B24}, 1,490,571 kg of H_2O are emitted. Here, no H_2 is emitted as this is not considered as a final emission in literature.

Fig. 10a shows the Ariane 6 black carbon emissions profile. The methodology used for all calculation approaches is the same which is why all lines overlap and lead to 2,078 kg. The other approach for Falcon considering a gas generator discussed in section 4.3 is giving black carbon emissions at nozzle exit level.

However, in the final emissions this black carbon no longer appears, as everything is assumed to be burned in the post-combustion according to the CEA methodology. According to the approach from James et al. (2021) black carbon also remains after post-combustion. This is in line with measurements and images from launches. However, the particle size distribution of these emissions is still unclear, but important for answering the question of lifetime in the atmosphere and potential climate impact (Maloney et al., 2022, 2025).

Fig. 10a also shows the Ariane 6 Al_2O_3 emissions. All calculation approaches have similar results (98,957 - 99,001 kg). The CEA method also yields small amounts of minor emissions depending on post-combustion which are not shown here (e.g. AlCl, $AlCl_2$, $AlCl_3$, AlO, AlOCl, AlOH, AlOHCl, $AlOHCl_2$, $Al(OH)_2Cl$, $Al(OH)_3$). The emission index approach EI_{B24} leads to slightly lower (90,462 kg) Al_2O_3 emissions.

https://doi.org/10.5194/egusphere-2026-3050
Preprint. Discussion started: 30 June 2026

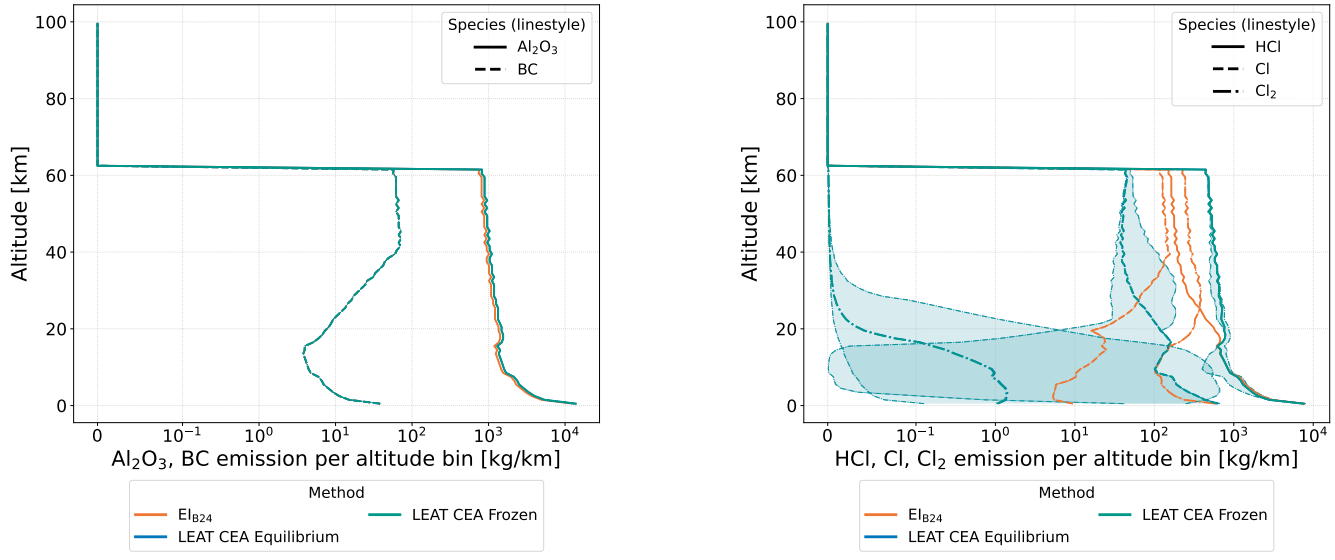

(a) Al_2O_3 and BC

(b) HCl, Cl, and Cl_2

Figure 10. Final emission of Ariane 6 launch depending on altitude shown for different calculation methodologies. Areas represent x_{ab} = 1.2 - 8, lines represent x_{ab} = 2. Decline at lower altitude represents thrust reduction. CEA equilibrium (blue), CEA frozen (green) and Cantera (red) approaches are overlapping for Al_2O_3 and BC. Al_2O_3 is showing no variability with changing factor. BC is calculated using the same approach for every calculation methodology. CEA equilibrium (blue), CEA frozen (green) approaches are overlapping for HCl, Cl and Cl_2. HCl variability is low except first 20 km. Cl_2 is declining with altitude, Cl varies compared with literature values.

Fig. 10b shows the chlorine species HCl, Cl, and Cl_2. In total between 45,443 - 56,824 kg of HCl, 1,471 - 8,734 kg of Cl and 1 - 7,634 kg of Cl_2 are emitted according to the three methodologies compared to 38,685 kg of HCl, 4,896 kg of Cl and 16,268 kg of Cl_2 with the emission index approach EI_{B24}. The amount of total chlorine species is comparable in this case. Emission indices may yield inaccurate values as they are fixed for a specific type of propellant.

5 Discussion

5.1 Mass profiles

The altitude-over-time profile calculated with LEAT compared to available launch vehicle data shows a maximum difference of a few kilometres for orbital launches. As the calculated trajectory, stage separation time and altitude were adjusted for the case studies to the actual flight data the calculated amount of propellant burned within an altitude interval should be representative of the actual mass flows. However, each individual launch is adjusted with respect to propellant mass, burn time, inclination, and stage separation so that for a detailed individual mass profile the individual data of the launch would be needed. If there is no trajectory data available (this is the case for most of the launches), the point of the pitchover manoeuvre and thrust reduction

https://doi.org/10.5194/egusphere-2026-3050
Preprint. Discussion started: 30 June 2026

needs to be estimated based on comparable launch systems or best guesses from the user. This introduces uncertainties to the mass profile calculations, which we will examine in more detail in the second part of the paper. The most commonly used mass profile in the literature comes from the publication by Ross and Sheaffer (2014; their Fig. 1) and was used by Ross and Sheaffer (2014); Ryan et al. (2022); Barker et al. (2024) - partly in adapted versions accounting for different stages. The only exception is Pradon et al. (2023), who calculated individual trajectories. We used a mass profile derived from Ross and Sheaffer (2014) for comparison with results directly obtained from LEAT. The profile from Ross and Sheaffer (2014) was calculated by multiplying the share of propellant mass given with the total individual launch vehicle propellant. Ross and Sheaffer (2014) is based on a mixture of the mass profiles for U.S. rockets excluding solid boosters. This explains the increase in mass at an altitude of 50-65 km. This is a typical altitude for booster separation (see, for example, the Ariane 62 flight). Once the booster mass flow is no longer subtracted, the share of mass flow rises. In the profile from Ross and Sheaffer (2014) one third (one half) of the total exhaust occurs within the lowest 20 (50) km. A comparison of the mass profile with the mass profiles calculated by LEAT shows that the mass is underestimated for lower altitudes up to 50 km. The thrust reduction and mass decrease are also not taken into account. For exhaust above this altitude, the generic profile derived from Ross and Sheaffer (2014) greatly overestimates the actual emissions. The same statement applies to the Starship launch, except for the first altitude bin (where the calculated emission is slightly lower), as well as to the Ariane profile. As already discussed by Ross and Sheaffer (2014), individual mass profiles may vary. Our comparison shows that there are significant differences that depend on the launch vehicle and launch trajectory. Therefore, customized profiles should be used whenever possible, provided that they can be reproduced from data.

5.2 Exhaust composition at the nozzle exit

Comparing the exhaust composition at the nozzle exit shows differences between the calculation approaches. First, there is a difference in the CEA frozen vs. equilibrium approach. For liquid engines with the gas generator taken into account, the equilibrium approach leads to a wider variation in species. However, the difference between species is different here; the frozen approach yields a few more species in the per mille range, which have a significantly lower share in the equilibrium case. For engines without a gas generator CEA equilibrium and CEA frozen yield the same number of species, but different species compositions. The cutoff was set to a mass fraction of 1^{-10} in all cases. For solid propellants, the equilibrium case leads to more species. For liquid engines, this could be explained with the longer reaction time, which also takes place in the nozzle. This is consistent with the higher proportion of oxygen still present in the CEA frozen case. Here, it appears that no complete reaction has taken place up to the nozzle throat. Furthermore, the proportion of CO_2 is significantly higher in the equilibrium case compared to the frozen case. For H_2O and H_2, however, the difference is not as significant; here, similar amounts are present in all cases. The differences between CEA equilibrium and CEA frozen can mainly be seen for minor exhaust species like OH and H. Here the frozen approach shows a wider variability regarding the types of minor species occurring (e.g. HCO, HO_2, etc.) at higher mass fractions in the per mille area and smaller fractions of the main exhaust species at the same total mass. Furthermore, a relatively large amount of O_2 and O compared to the equilibrium case is present at the exit. When considering a gas generator with additional exhaust flow there are some remarkable deviations for the exhaust of BC, C_2H_6 and CH_4. These

https://doi.org/10.5194/egusphere-2026-3050
Preprint. Discussion started: 30 June 2026

additional emissions occur due to fuel-rich burning in the gas generator and do not occur in such large amounts in the main engine. It is noteworthy that the amount of BC from this calculation leads to almost the same amount as proposed by James et al. (2021). The Cantera approach is exactly in agreement with the CEA equilibrium calculation without gas generator and therefore provides a good alternative if no CEA licence is available.

For the solid booster, only the CEA approach is shown as Cantera is not implemented for solid phase of solid propellants exhaust. Also here, the variety of exhaust species differs between the approaches. It should be noted that the frozen approach here also takes into account a freezing point of the reactions at the nozzle exit level as for a freezing point within the throat no results can be obtained. For the solid engine, the equilibrium approach produces a slightly greater variety of minor exhaust species. For the main exhaust species and other species down to 0.01% the results show good consistency. The variety of exhaust species from the solid engine is much higher than for liquid engines representing the complexity of aluminium and chlorine species reactions. Compared to the approach from James et al. (2021), BC is not present in the CEA exhaust calculation. This represents a limitation of the tool as, except for very low oxidizer-to-fuel mass ratios, no BC formation can be calculated with CEA or Cantera.

The exact proportional distribution of exhaust species and the species considered varies between sources for the same type of propellant, based on the assumptions and engine parameters the authors considered. The comparison is listed in the supplementary material in Sect. S1.2. These studies therefore do not account for engine-specific parameters such as mixture ratio or nozzle expansion ratio. As the results for the equilibrium vs. frozen approaches showed, this can lead to different results. In particular, the mixture ratio should be individually adjusted for each engine, as this has a significant influence on the composition of the exhaust. Furthermore, a large number of species are not considered that can have an influence on the following post-combustion reactions.

5.3 Emission profiles

For emissions including post-combustion, the examples show that the main emissions like CO_2 and H_2O do not vary significantly when changing the uncertainty factor for the methodologies of Cantera or CEA. In comparison to that, the minor species like CO, H_2, NO and OH have a particularly large margin of uncertainty due to the variation in the uncertainty factor. They are therefore highly dependent on the chosen post-combustion mass flow represented via the uncertainty factor x_{ab}. While the uncertainty range is comparable between CEA equilibrium and frozen, there is a significant difference to Cantera. We assume that this is due to the different approaches used to calculate at constant enthalpy and pressure. While CEA uses an adapted c_{p}, whereas the value used by Cantera remains constant. Therefore with a given enthalpy and pressure, changes in temperature differ. With a constant c_{p} the post-combustion temperature is higher and therefore leads to larger amounts of the temperature-driven NO formation. Therefore Cantera represents the worst case with the highest amounts of NO formed. Furthermore, less dissociation occurs which explains e.g. the difference in OH. OH is currently not considered at all in ozone modelling of launch emissions but does interact with CH_4 and O_3.

For Al_2O_3 there is no difference at all when comparing the different calculation approaches. This is due to already fully oxidized Al, and no new reactions occur during post-combustion.

https://doi.org/10.5194/egusphere-2026-3050
Preprint. Discussion started: 30 June 2026

The exact amount of Cl, Cl_2 or HCl can make a difference when considering emissions in global modelling as they affect the reactions with each other on the one hand and with ozone on the other. HCl is an inactive chlorine reservoir species, whereas Cl is immediately reactive and Cl_2 can be activated by photodissociation. From the results it can be seen that with less post-combustion, less Cl_2 and more Cl is formed. Chlorine can react multiple times with O_3 before becoming a reservoir species, such as chlorine nitrate ($ClONO_2$) or HCl. Therefore, differentiated emission inventories can have have a significant impact on simulated ozone depletion. The variation is again very similar for CEA frozen and equilibrium. Especially for Cl and Cl_2 there is a large range of uncertainty, but not for HCl, where the variations are lower.

For comparison with emissions the most sophisticated approach in the literature, by Barker et al. (2024) to calculate altitude-dependent emission indices (hereafter referred to as EI_{B24}) was used for the different propellants and primary emission indices depending on the selected fuel. For this, the secondary emission indices are calculated as altitude-dependent values and multiplied with the calculated trajectory mass profile. It must be taken into account that the mass profiles of Barker et al. (2024) are not used for comparison, only the emission calculation, so this analysis represents the sensitivity of emissions with respect to the emission calculation method and not with respect to the mass profile. For CO_2 the LEAT calculations show lower emissions compared to altitude-dependent emission indices (29.0%-67.84%), whereas CO is higher by 518.3% - 1351.7% in LEAT than for EI_{B24}. This is especially visible up to an altitude of 40 km where the LEAT calculations show less post-combustion than assumed with EI_{B24}. For higher altitudes than 75 km, EI_{B24} gives results that lie between the CEA equilibrium and frozen approach for CO. In total, all methodologies lead to a conserved carbon budget. In the case of H_2O, the approach with altitude-depended emission indices leads to a higher amount of H_2O emission (89.9% - 93.5% LEAT compared to EI_{B24}). But it is important to mention that when also assuming full combustion of present H_2 with a mass conversion factor of 9 from H_2 to H_2O the total mass in H_2O is comparable with EI_{B24}. The NOx emission calculated with altitude-depended emission indices interestingly shows emissions at altitudes below 5 km in the order of the Cantera approach but then fall below the CEA method already below 10 km. The variance is therefore very high, from 0.0082% to 644.3% in total mass, comparing LEAT to EI_{B24}. For the case of Al_2O_3 the approach with altitude-depended emission indices leads to a bit smaller amounts of emission (109.4% LEAT), but this depends on the assumed percentage of aluminium within the propellant. For BC the results are the same because the same approach was used from James et al. (2021).

For chlorine species, the CEA approach yields higher amounts than the EI_{B24} approach Barker (2024) for HCl (117.5% - 146.9%). For Cl (30.0% - 178.1%) the range is broader. Total Cl_2 emissions are lower (0.0% - 46.1%) with LEAT. It should be noted here that Cl_2 emissions decrease with increasing altitude in LEAT, while they increase in the EI_{B24} approach. For HCl, there is good agreement in the first 20 km, while for EI_{B24} they decrease significantly thereafter and Cl and Cl_2 are formed instead.

In order to show the different emission calculation approaches and additionally the progress of the LEAT tool compared to previously used methodologies a comparison of various emission inventories is shown in Tab. 4. This publication presents the first publicly available tool for calculating emission inventories. Both trajectories and emissions are calculated within LEAT for each launch system. The mass profile is calculated from the inventories in Pradon et al. (2023), which used optimized trajectories for launch vehicles with fixed profiles. In LEAT, on the other hand, the flight paths for each launch system can be

https://doi.org/10.5194/egusphere-2026-3050
Preprint. Discussion started: 30 June 2026

calculated individually, or the user can provide their own trajectories. Compared to published inventories, which only consider a certain number of propellants, the LEAT tool is therefore largely independent in the choice of propellant and launch vehicle. This is also reflected in the representation of exhaust and emission species. When using LEAT, the user theoretically has access to the entire thermo.lib file with over 2000 species. The literature values are based on the assumption of a fixed combustion within rocket engines. In comparison, LEAT calculates exhaust composition based on engine parameters. Except for James et al. (2021); Barker et al. (2024) and Vliex et al. (2026), altitude-dependent changes are not taken into account. Emissions of NOx due to post-combustion are mostly derived from air-breathing engines from aviation based on Larson et al. (2017) and are therefore not accurate. James et al. (2021) used simulated values. Although there are still uncertainties regarding the reacting atmospheric mass during post-combustion, LEAT considers altitude-dependent combustion reactions specifically for the atmospheric composition at the date and location of the launch. Furthermore, the comparison above shows the advantage of the tool as it can also calculate, e.g., OH and additional emission species which are not represented within existing emission methods as final emissions. As emissions significantly influence the effects on climate and ozone (Ryan et al., 2022; Maloney et al., 2022) precise information on the location, type, and fraction of emission species is needed. This gap in the literature is therefore addressed by LEAT.

5.4 Limitations

Calculating emissions from the space sector is still in its early stages, hence there is a need for further research to close existing knowledge gaps. Partly, these gaps are filled by LEAT by providing a transparent tool for launch vehicle-based emission calculations. However, some uncertainties still remain. For example, accurate trajectory calculation relies on mission-specific values. Furthermore the mixing between engine exhaust and surrounding air is subject to significant uncertainties. These are represented by parameter-dependent modelling within LEAT. New findings and measurements could refine these parameters. The tool therefore has the potential to refine the emission calculation in the future. CFD simulations would allow better estimation of the actual intake of ambient atmospheric air and could therefore be useful to refine the simplified models within this tool. Furthermore, ground-based measurements as well as within the troposphere and stratosphere would provide real insight into altitude-dependent post-combustion processes and allow to compare the modelled emission data with real emissions. Both approaches offer local insights into the complex altitude and location-dependent processes of post-combustion. However, multiple such data points along a trajectory would be needed for a precise statement of the processes. Currently, the tool does not cover the recovery of core stages during the launch phase. This should be implemented in an updated version of LEAT in the future.

https://doi.org/10.5194/egusphere-2026-3050
Preprint. Discussion started: 30 June 2026

Table 4. Overview of contemporary launch emission inventories and the new tool LEAT. All inventories incorporate stage-dependent information.

Emission inventory/tool	Ryan et al. (2022)[a]	Pradon et al. (2023)[b]	Barker et al. (2024)	Brown et al. (2024)	Vliex et al. (2026)	Fischer et al. (2026)
propellant combinations	kerosene, LH2, hypergolic, solid	kerosene, LH2, hypergolic, solid	kerosene, LH2, hypergolic, solid, LCH4	kerosene, LH2, hypergolic, solid	kerosene, LH2, hypergolic, solid	all propellants
Mass profile	based on Ross and Sheaffer (2014; Fig. 1)	optimized launch-vehicle-dependent trajectory	based on Ross and Sheaffer (2014; Fig. 1)	linear[c] up to 50 km, followed by exponential decay	launch-vehicle-dependent trajectory with fiyxed gravity turn	launch-vehicle-dependent trajectory
Emission indices	propellant-dependent emission indices from literature	stoichiometric assumption	propellant-dependent emission indices from literature partly modified by parametrized post-combustion	propellant-dependent emission indices from literature	engine-dependent exhaust and altitude depended emission indices from literature	various options incl. chemical equilibrium with post-combustion (parametrized for black carbon)
Exhaust species	H_2O, BC, Al_2O_3, HCl, Cl, NO_x	H_2O , CO_2, Al_2O_3, Chlorine[d]	H_2O, H_2, CO, CO_2, NO_x, BC, Al_2O_3, HCl, Cl, Cl_2	H_2O, CO_2, NO_x, BC, Al_2O_3, Cl_x[e]	H_2O, H_2, CO, CO_2, NO_x, BC, Al_2O_3, HCl, Cl, Cl_2	>2000 species[f]
Altitude	up to 80 km (model top)	up to 100 km	up to 80 km	up to 80 km (focus on 15-50 km)	up to 80 km	up to 1000 km[g]

(a) Ryan et al. (2022) build a scenario based on 5.6%/yr increase and also a space tourism scenario.

(b) Pradon et al. (2023) state that they capture about 77% of all launches in the respective period.

(c) Likely this means that the values are constant throughout the first 50 km.

(d) Pradon et al. (2023) show HCl emission indices but refer to "chlorine" emissions throughout the text.

(e) Show HCl as emitted species (see their Table 1; and respective annotation) but refer to "reactive chlorine" throughout the text.

https://doi.org/10.5194/egusphere-2026-3050
Preprint. Discussion started: 30 June 2026

(f) NASA CEA's thermo.lib database

(g) Limit of the atmospheric model. As upper stages are actively controlled, the practical limit is about 150 km

6 Conclusions and outlook

Emission inventories are necessary in order to calculate the effects of rocket launches on the climate and ozone. With more precise modelling inputs, locally and temporally varying effects can be taken into account.

For the calculation of emission inventories of rocket launches we developed the Launch Emission Assessment Tool (LEAT). LEAT combines the calculation of launch-specific trajectories with engine-specific and trajectory-dependent emission calculation. The trajectory calculation provides information on where and when how much propellant was burned. The emission calculation allows the determination of emission species and quantity.

In comparison to previous studies, LEAT allows the calculation of individual emission profiles for each specific launch vehicle and launch. The individual rocket-specific mass profiles vary significantly from the generic profiles used in previous studies. Comparisons of the trajectories calculated with LEAT show good agreement with launch data extracted from video streams. Custom trajectories can also be used.

Compared to existing emission inventories, launch vehicle- and engine-specific parameters like geometry, propellant mixture ratio and nozzle expansion ratio are taken into account as well as local and temporal changes within the atmosphere. With this, spatially and temporally resolved emission inventories can be built containing more detailed information on the composition (type and quantity) of the emissions.

LEAT offers three emission calculation methodologies. The first uses a set of fixed emission indices from a database, which contains various sets of emission indices from previous publications. These represent the final emissions after interaction with the atmosphere. Those values are only dependent on propellant and vary with altitude in only one case. The second and most detailed emission calculation method within LEAT uses the CEA software (requires additional free licence provided by NASA) in a two-step process: (i) exhaust at nozzle exit level is calculated assuming either equilibrium or frozen chemistry, (ii) mixing with the surrounding atmosphere and post-combustion is calculated assuming a constant enthalpy and pressure. As an open-source alternative, the third methodology is using the Python implementation of Cantera which follows the same two-step approach considering engine exhaust and post-combustion as the CEA methodology. Our results show that at the nozzle exit the Cantera and CEA equilibrium approach produce similar results.

The latter two emission calculation methodologies are based on one-dimensional chemistry, which enables rapid calculation of emissions but does not reflect local differences within the exhaust gas plume. To account for post-combustion for CEA and Cantera, the uncertainty factor x_{ab} regulates the mass flow from the surrounding atmosphere. For the final emissions, the selected case studies show that the main emissions like CO_2 and H_2O do not vary significantly when changing the uncertainty factor for the methodologies of Cantera or CEA. In contrast, the minor species like CO, H_2, NO and OH have a relatively large margin of uncertainty due to the variation in the uncertainty factor. Compared to existing inventories, calculations with LEAT also produce additional minor species which affect ozone chemistry (e.g. OH). The implemented calculation parameters allow

https://doi.org/10.5194/egusphere-2026-3050
Preprint. Discussion started: 30 June 2026

uncertainties in the emission calculation to be taken into account; however, additional CFD and measurement data are required for a more accurate determination. When creating comprehensive inventories these input parameters (e.g. gravity turn, mass flow of surrounding air) represent an uncertainty in the inventory results. These will be analysed in more detail in a second paper.

Based on the tool, launch emission inventories are currently being developed for the years 2019-2025. The tool can also be used for future launch scenarios to calculate the impact of different launch vehicle, propellant, and trajectory choices. The field of application ranges from developing emission inventories for global modelling and research to calculating emissions within life cycle assessment (LCA) or a multidisciplinary design optimization (MDO) for eco-designing launch vehicles. For this, coupling with a response model of the emission impacts would be needed. Finally, the creation of reports for the consideration of environmental regulations is also possible, for example for ESA LCA studies or PEFCR4space EC DG DEFIS (2026), frameworks for the environmental reporting of space industry.

LEAT is the first open-source emission calculation tool for rocket launch emissions that calculates individual launches and their emissions depending on the launch vehicle and trajectory. Emissions from future launch systems with new propellant combinations can also be simulated in this way. LEAT enables the therefore user to develop own trajectory and emission inventories as a basis for estimating the (global) effects of rocket launch emissions.

Code and data availability. The exact version 1.0 of LEAT described in this paper is licensed under the terms of the GNU Affero General Public License 3.0 and can be obtained under https://doi.org/10.5281/zenodo.20643441 (Fischer et al., 2026). Additional needed python packages can be installed using pip with the requirements.txt file provided in the repo. The additional free licence for CEA can be requested under https://software.nasa.gov/software/LEW-17687-1.

Data availability. Used input and output data for the shown case studies calculation within this paper can be obtained as additional files under https://doi.org/10.5281/zenodo.20643871 (Fischer, 2026) licensed under CC-BY-4.0.
Data from McDowell (2026) used to derive launch logs can be derived from https://planet4589.org/space/gcat under CC-BY.

Author contributions. Jan-Steffen Fischer has written the code (with support from Sebastian Winterhoff) and contributed with text writing, figure plotting and formatting. Stefanos Fasoulas contributed with fundraising and scientific guidance. Matthias Nützel contributed with text writing, paper conceptualization and structure as well as reviewing during and after the writing process. Anja Schmidt contributed with paper conceptualization and structure as well as reviewing the paper draft.

Competing interests. The authors declare that no competing interests are present.

https://doi.org/10.5194/egusphere-2026-3050
Preprint. Discussion started: 30 June 2026

Acknowledgements. The authors would like to thank Connor Barker for his detailed answers to our questions about his approach.

The authors would like to gratefully acknowledge funding by the German Space Agency DLR, funding reference 50RL2180 from the Federal Ministry for Economic Affairs and Climate Action of Germany based on a decision of the German Bundestag.

Generative Artificial Intelligence was used by the authors to correct the text. The authors take full responsibility for the content of the publication.

https://doi.org/10.5194/egusphere-2026-3050
Preprint. Discussion started: 30 June 2026

References

Alexeenko, A. A., Gimelshein, N. E., Levin, D. A., Collins, R. J., Rao, R., Candler, G. V., Gimelshein, S. F., Hong, J. S., and Schilling, T.: Modeling of Flow and Radiation in the Atlas Plume, Journal of Thermophysics and Heat Transfer, 16, 50–57, https://doi.org/10.2514/2.6651, 2002.

Arianespace: Ariane flight VA263 videostream, https://www.youtube.com/watch?v=yvvUCkAUqvI, 2025.

Barker, C.: cbarker211/Satellite-Megaconstellation-Emission- Inventory-Development: Satellite Megaconstellation Emission Inventory v1.0.0, https://doi.org/10.5281/zenodo.13136857, 2024.

Barker, C. R., Marais, E. A., and McDowell, J. C.: Global 3D Rocket Launch and Re-Entry Air Pollutant and CO2 Emissions at the Onset of the Megaconstellation Era, Scientific Data, 11, 1079, https://doi.org/10.1038/s41597-024-03910-z, 2024.

Barker, C. R., Marais, E. A., Tan, E. Y. P., Eastham, S. D., Diskin, G. S., DiGangi, J. P., Choi, Y., Rollins, A. W., Waxman, E., Bui, T. P., Gatebe, C. K., Dean-Day, J., and Poudyal, R.: Radiative Forcing and Ozone Depletion of a Decade of Satellite Megaconstellation Missions, Earth's Future, 14, e2025EF007 229, https://doi.org/10.1029/2025EF007229, 2026.

Bauer, C., Koch, A., Minutolo, F., and Grenard, P.: Engineering Model for Rocket Exhaust Plumes Verified by CFD Results, in: 29th International Symposium on Space Technology and Science, Nagoya, Japan, 2013.

Bennett, R. and McDonald, A.: Recent activities and studies on the environmental impacts of rocket effluents, in: 34th AIAA/ASME/SAE/ASEE Joint Propulsion Conference and Exhibit, https://doi.org/10.2514/6.1998-3850, 1998.

Billington, C. J.: Starship telemetry tool under MIT licence, https://github.com/chrisjbillington/starship_telemetry/, 2023.

Brown, T. F. M., Bannister, M. T., Revell, L. E., Sukhodolov, T., and Rozanov, E.: Worldwide Rocket Launch Emissions 2019: An Inventory for Use in Global Models, Earth and Space Science, 11, e2024EA003 668, https://doi.org/10.1029/2024EA003668, 2024.

Cziczo, D. J., Murphy, D. M., Thomson, D. S., and Ross, M. N.: Composition of Individual Particles in the Wakes of an Athena II Rocket and the Space Shuttle, Geophysical Research Letters, 29, https://doi.org/10.1029/2002GL015991, 2002.

Daehnick, C., Gang, J., and Rozenkopf, I.: Space Launch: An Oversupply or a Shortfall?, Tech. rep., McKinsey & Company, 2023.

Danilin, M. Y., Popp, P. J., Herman, R. L., Ko, M. K. W., Ross, M. N., Kolb, C. E., Fahey, D. W., Avallone, L. M., Toohey, D. W., Ridley, B. A., Schmid, O., Wilson, J. C., Baumgardner, D. G., Friedl, R. R., Thompson, T. L., and Reeves, J. M.: Quantifying Uptake of HNO_3 and H_2O by Alumina Particles in Athena-2 Rocket Plume, Journal of Geophysical Research: Atmospheres, 108, 2002JD002 601, https://doi.org/10.1029/2002JD002601, 2003.

EC DG DEFIS: Product Environmental Footprint Category Rules (PEFCR) for the space sector, https://defence-industry-space.ec.europa.eu/eu-space/product-environmental-footprint-category-rules-pefcr-space-sector_en, 2026.

Ecker, T., Karl, S., and Hannemann, K.: Combustion Modeling in Solid Rocket Motor Plumes, in: 8th European Conference for Aeronautics and Aerospace Sciences (EUCASS), p. 17 pages, [object Object], Madrid, Spanien, https://doi.org/10.13009/EUCASS2019-79, 2019.

Emmert, J. T., Drob, D. P., Picone, J. M., Siskind, D. E., Jones, M., Mlynczak, M. G., Bernath, P. F., Chu, X., Doornbos, E., Funke, B., Goncharenko, L. P., Hervig, M. E., Schwartz, M. J., Sheese, P. E., Vargas, F., Williams, B. P., and Yuan, T.: NRLMSIS 2.0: A Whole-Atmosphere Empirical Model of Temperature and Neutral Species Densities, Earth and Space Science, 8, e2020EA001 321, https://doi.org/10.1029/2020EA001321, 2021.

Fischer, J.-S.: Supplementary Files to Launch Emission Assessment Tool (LEAT v1.0): Part I - Development of a tool to calculate altitude-dependent rocket launch emissions for use in chemistry-climate models, https://doi.org/10.5281/zenodo.20643871, 2026.

https://doi.org/10.5194/egusphere-2026-3050
Preprint. Discussion started: 30 June 2026

Fischer, J.-S., Winterhoff, S., and Fasoulas, S.: Launch Emission Assessment Tool (LEAT v1.0), https://doi.org/10.5281/zenodo.20643441, 2026.

Fleeman, E. L.: Missile Design Guide, American Institute of Aeronautics and Astronautics, Inc., Reston, VA, https://doi.org/10.2514/4.106347, 2001.

Gomberg, R. I. and Stewart, R. B.: A Computer Simulation of the Afterburning Processes Occurring within Solid Rocket Motor Plumes in the Troposphere, NASA Technical Note NASA-TN-D-8303, NASA Langley Research Center, Hampton, VA, United States, 1976.

Goodwin, D. G., Moffat, H. K., Schoegl, I., Speth, R. L., and Weber, B. W.: Cantera: An Object-oriented Software Toolkit for Chemical Kinetics, Thermodynamics, and Transport Processes, https://www.cantera.org, https://doi.org/10.5281/zenodo.14455267, version 3.1.0, 2024.

Gordon, S. and McBride, B. J.: Computer Program for Calculation of Complex Chemical Equilibrium Compositions and Applications. Part 1: Analysis, Tech. Rep. 1311, NASA Lewis Research Center, Cleveland, OH, United States, 1994.

Herget, W. F.: An Instrumentation System to Study Rocket Exhaust Plume Radiative Processes Final Report, Tech. Rep. NASA-CR-68540, 1965.

Huzel, D. K. and Huang, D. H.: Modern Engineering for Design of Liquid-Propellant Rocket Engines, vol. 147 of *Progress in Astronautics and Aeronautics*, American Institute of Aeronautics and Astronautics, 1992.

Jain, A. K., Eastham, S. D., and Hastings, D.: Future of Satellite Reentry and Earth's Atmosphere: the Lifetime and Direct Radiative Forcing of Space Debris Reentry Alumina, ESS Open Archive, https://doi.org/10.22541/essoar.170110669.90121203/v1, 2023.

James, M. M., Lympany, S. V., Salton, A. R., Matthew F. Calton, Miake-Lye, R. C., and Wayson, R. L.: Commercial Space Vehicle Emissions Modeling, Transportation Research Board, Washington, D.C., https://doi.org/10.17226/26142, 2021.

Koch, A. D., Bauer, C., Dumont, E., Minutolo, F., Sippel, M., Grenard, P., Ordonneau, G., Winkler, H., Guénot, L., Linck, C., Wood, C. R., Vira, J., Sofiev, M., and Tarvainen, V.: Multidisciplinary Approach for Assessing the Atmospheric Impact of Launchers, in: 4th International Conference of the European Aerospace Societies (CEAS) Air & Space Conference, Linköping University Electronic Press, Linköping, Finnland, 2013.

Larson, E. J. L., Portmann, R. W., Rosenlof, K. H., Fahey, D. W., Daniel, J. S., and Ross, M. N.: Global Atmospheric Response to Emissions from a Proposed Reusable Space Launch System, Earth's Future, 5, 37–48, https://doi.org/10.1002/2016EF000399, 2017.

Lee, D., Fahey, D., Skowron, A., Allen, M., Burkhardt, U., Chen, Q., Doherty, S., Freeman, S., Forster, P., Fuglestvedt, J., Gettelman, A., De León, R., Lim, L., Lund, M., Millar, R., Owen, B., Penner, J., Pitari, G., Prather, M., Sausen, R., and Wilcox, L.: The contribution of global aviation to anthropogenic climate forcing for 2000 to 2018, Atmospheric Environment, 244, 117 834, https://doi.org/10.1016/j.atmosenv.2020.117834, 2021.

Leone, D. and Turns, S.: Active Chlorine and Nitric Oxide Formation from Chemical Rocket Plume Afterburning, in: 32nd Aerospace Sciences Meeting and Exhibit, American Institute of Aeronautics and Astronautics, Reno,NV,U.S.A., https://doi.org/10.2514/6.1994-788, 1994.

Maloney, C. M., Portmann, R. W., Ross, M. N., and Rosenlof, K. H.: The Climate and Ozone Impacts of Black Carbon Emissions From Global Rocket Launches, Journal of Geophysical Research: Atmospheres, 127, e2021JD036 373, https://doi.org/10.1029/2021JD036373, 2022.

Maloney, C. M., Portmann, R. W., Ross, M. N., and Rosenlof, K. H.: Investigating the Potential Atmospheric Accumulation and Radiative Impact of the Coming Increase in Satellite Reentry Frequency, Journal of Geophysical Research: Atmospheres, 130, e2024JD042 442, https://doi.org/https://doi.org/10.1029/2024JD042442, e2024JD042442 2024JD042442, 2025.

https://doi.org/10.5194/egusphere-2026-3050
Preprint. Discussion started: 30 June 2026

Mastrandrea, M. D., Christopher B. Field, Thomas F. Stocker, Ottmar Edenhofer, Kristie L. Ebi, David J. Frame, Hermann Held, Elmar Kriegler, Katharine J. Mach, Patrick R. Matschoss, Gian-Kasper Plattner, Gary W. Yohe, and Francis W. Zwiers: Guidance Note for Lead Authors of the IPCC Fifth Assessment Report on Consistent Treatment of Uncertainties, Tech. rep., Intergovernmental Panel on Climate Change (IPCC), 2010.

McDowell, J. C.: General Catalog of Artificial Space Objects Release 1.8.0 Data Update 2026 Mar 28 under CC-BY licence, planet4589.org/space/gcat, 2026.

Messerschmid, E. and Fasoulas, S.: Raumfahrtsysteme, Springer Berlin Heidelberg, https://doi.org/10.1007/978-3-662-49638-1, 2017.

Murphy, D. M., Abou-Ghanem, M., Cziczo, D. J., Froyd, K. D., Jacquot, J., Lawler, M. J., Maloney, C., Plane, J. M. C., Ross, M. N., Schill, G. P., and Shen, X.: Metals from Spacecraft Reentry in Stratospheric Aerosol Particles, Proceedings of the National Academy of Sciences, 120, e2313374 120, https://doi.org/10.1073/pnas.2313374120, 2023.

Nickerson, G. and Johnson, C.: A soot prediction model for the TDK computer program, in: 28th Joint Propulsion Conference and Exhibit, American Institute of Aeronautics and Astronautics, Nashville,TN,U.S.A., https://doi.org/10.2514/6.1992-3391, 1992.

Niemeyer, K.: Rocket Propulsion Notes, https://github.com/kyleniemeyer/rocket-propulsion, 2026.

Ocko, I. B. and Hamburg, S. P.: Climate consequences of hydrogen emissions, Atmospheric Chemistry and Physics, 22, 9349–9368, https://doi.org/10.5194/acp-22-9349-2022, 2025.

Paoli, R., Poubeau, A., and Cariolle, D.: Large-Eddy Simulations of a Reactive Solid Rocket Motor Plume, AIAA Journal, 58, 1639–1656, https://doi.org/10.2514/1.J058601, 2020.

Plastinin, Y., Karabadzhak, G., Khmelinin, B., Baula, G., and Rodionov, A.: Investigation of Soot Density in the LOX/Kerosene Engine Booster Exhaust of Atlas II and Atlas III from Remote Measurements of Radiation Intensity, in: 43rd AIAA Aerospace Sciences Meeting and Exhibit, American Institute of Aeronautics and Astronautics, Reno, Nevada, https://doi.org/10.2514/6.2005-769, 2005.

Popp, P. J., Ridley, B. A., Neuman, J. A., Avallone, L. M., Toohey, D. W., Zittel, P. F., Schmid, O., Herman, R. L., Gao, R. S., Northway, M. J., Holecek, J. C., Fahey, D. W., Thompson, T. L., Kelly, K. K., Walega, J. G., Grahek, F. E., Wilson, J. C., Ross, M. N., and Danilin, M. Y.: The Emission and Chemistry of Reactive Nitrogen Species in the Plume of an Athena II Solid-fuel Rocket Motor, Geophysical Research Letters, 29, https://doi.org/10.1029/2002GL015197, 2002.

Poubeau, A.: Simulation des émissions d'un moteur à propergol solide : vers une modélisation multi-échelle de l'impact atmosphérique des lanceurs, Ph.D. thesis, Université Toulouse 3 Paul Sabatier, Toulouse, France, 2015.

Pradon, C. V. M., Eastham, S. D., Chossière, G., Sabnis, J., Speth, R. L., Barrett, S. R. H., and André Jooste, J.: Global Three-Dimensional Emission Inventory for Launch Vehicles from 2009 to 2018, Journal of Spacecraft and Rockets, 60, 716–727, https://doi.org/10.2514/1.A35385, 2023.

Ross, M., Toohey, D., Peinemann, M., and Ross, P.: Limits on the Space Launch Market Related to Stratospheric Ozone Depletion, 7, 50–82, https://doi.org/10.1080/14777620902768867, 2009.

Ross, M., Mills, M., and Toohey, D.: Potential Climate Impact of Black Carbon Emitted by Rockets, Geophysical Research Letters, 37, 2010GL044 548, https://doi.org/10.1029/2010GL044548, 2010.

Ross, M. N. and Sheaffer, P. M.: Radiative Forcing Caused by Rocket Engine Emissions, Earth's Future, 2, 177–196, https://doi.org/10.1002/2013EF000160, 2014.

Ross, M. N., Benbrook, J. R., Sheldon, W. R., Zittel, P. F., and McKenzie, D. L.: Observation of Stratospheric Ozone Depletion in Rocket Exhaust Plumes, Nature, 390, 62–64, https://doi.org/10.1038/36318, 1997.

https://doi.org/10.5194/egusphere-2026-3050
Preprint. Discussion started: 30 June 2026

Rudman, S.: Determination of Soot Concentration from Atlas Flight Data, in: Proc. 21st JANNAF Exhaust Plume Technology Meeting, 1994.

Ryan, R. G., Marais, E. A., Balhatchet, C. J., and Eastham, S. D.: Impact of Rocket Launch and Space Debris Air Pollutant Emissions on Stratospheric Ozone and Global Climate, Earth's Future, 10, e2021EF002 612, https://doi.org/10.1029/2021EF002612, 2022.

Schmid, O., Reeves, J. M., Wilson, J. C., Wiedinmyer, C., Brock, C. A., Toohey, D. W., Avallone, L. M., Gates, A. M., and Ross, M. N.: Size-resolved Particle Emission Indices in the Stratospheric Plume of an Athena II Rocket, Journal of Geophysical Research: Atmospheres, 108, 2002JD002 486, https://doi.org/10.1029/2002JD002486, 2003.

Sheaffer, P.: Garbage-In Garbage-Out (GIGO): The Use and Abuse of Combustion Modeling and Recent U.S. Spacelaunch Environmental Impacts, in: Earth and Space Science Open Archive, https://doi.org/10.1002/essoar.10509138.3, 2021.

Simmons, F.: Rocket Exhaust Plume Phenomenology, American Institute of Aeronautics and Astronautics, Inc., Washington, DC, https://doi.org/10.2514/4.989087, 2000.

Sirieys, E., Gentgen, C., Milton, J., and De Weck, O.: Space Sustainability Isn't Just about Space Debris: On the Atmospheric Impact of Space Launches, MIT Science Policy Review, 3, 143–151, https://doi.org/10.38105/spr.whfig18hta, 2022.

SpaceX: Starlink 4-23 mission videostream, https://www.youtube.com/watch?v=07RGJ04HRns, 2022.

SpaceX: Starship IFT-8 videostream, https://x.com/SpaceX/status/1896909928381768044, 2025.

Stevens, M. H., Gumbel, J., Englert, C. R., Grossmann, K. U., Rapp, M., and Hartogh, P.: Polar mesospheric clouds formed from space shuttle exhaust, Geophysical Research Letters, 30, 2003GL017 249, https://doi.org/10.1029/2003GL017249, 2003.

Stevens, M. H., Meier, R. R., Chu, X., DeLand, M. T., and Plane, J. M. C.: Antarctic mesospheric clouds formed from space shuttle exhaust, Geophysical Research Letters, 32, 2005GL023 054, https://doi.org/10.1029/2005GL023054, 2005.

Stewart, R. B. and Gomberg, R. I.: The Production of Nitric Oxide in the Troposphere as a Result of Solid-Rocket-Motor Afterburning, Tech. Rep. NASA TN D-8137, Langley Research Center, Hampton, VA, USA, 1976.

Stryjewski, J.: Soot mass loading and particle size effects on laser backscatter from rocket plumes, in: 39th Aerospace Sciences Meeting and Exhibit, American Institute of Aeronautics and Astronautics, Reno,NV,U.S.A., https://doi.org/10.2514/6.2001-356, 2001.

Sutton, G. P. and Biblarz, O.: Rocket Propulsion Elements, John Wiley & Sons Inc, Hoboken, New Jersey, ninth edition edn., 2017.

Troyes, J., Dubois, I., Borie, V., and Boischot, A.: Multi-Phase Reactive Numerical Simulations of a Model Solid Rocket Exhaust Jet, in: 42nd AIAA/ASME/SAE/ASEE Joint Propulsion Conference & Exhibit, American Institute of Aeronautics and Astronautics, Sacramento, California, https://doi.org/10.2514/6.2006-4414, 2006.

Vliex, Y. S. W., van 't Hoff, J. A., and Dedoussi, I. C.: The Role of Propellant Type, Re-Entry, and Plume Reactions in the Atmospheric Impacts of Spaceflight, Earth's Future, 14, e2025EF007 795, https://doi.org/https://doi.org/10.1029/2025EF007795, e2025EF007795 2025EF007795, 2026.

Voigt, C., Schumann, U., and Graf, K.: Contrail formation in the tropopause region caused by emissions from an Ariane 5 rocket, in: Progress in Propulsion Physics, edited by Calabro, M., DeLuca, L., Frolov, S., Galfetti, L., and Haidn, O., pp. 183–196, EDP Sciences, Munich, Germany, https://doi.org/10.1051/eucass/201608183, 2016.

Weisenstein, D. K., Keith, D. W., and Dykema, J. A.: Solar Geoengineering Using Solid Aerosol in the Stratosphere, Atmospheric Chemistry and Physics, 15, 11 835–11 859, https://doi.org/10.5194/acp-15-11835-2015, 2015.

World Meteorological Organization (WMO): Scientific Assessment of Ozone Depletion: 2022, 2022.